Geochemistry, Geophysics, Geosystems®

RESEARCH ARTICLE
10.1029/2024GC011691

A Comparative Study of Cave System Calcium Isotope Ratios: Implications for Quantitative Reconstruction of Paleorainfall From Speleothems

Cameron B. de Wet[1,2,3], Elizabeth M. Griffith[4], Andrea M. Erhardt[5], and Jessica L. Oster[2]

[1]Department of Earth and Climate Sciences, Middlebury College, Middlebury, VT, USA, [2]Department of Earth and Environmental Sciences, Vanderbilt University, Nashville, TN, USA, [3]Department of Earth and Planetary Sciences, University of California, Davis, Davis, CA, USA, [4]School of Earth Sciences, The Ohio State University, Columbus, OH, USA, [5]Department of Earth and Environmental Sciences, University of Kentucky, Lexington, KY, USA

Key Points:

- Drier periods correspond to higher Ca isotope ratios and more prior calcite precipitation, though there is variability between drip sites
- Modern calcite trace element ratios positively correlate with Ca isotope data at one of the two cave sites
- Ca isotope data provides an independent constraint on water infiltration to aid the interpretation of other hydrologically sensitive proxies

Supporting Information:

Supporting Information may be found in the online version of this article.

Correspondence to:

C. B. de Wet,
cdewet@ucdavis.edu

Citation:

de Wet, C. B., Griffith, E. M., Erhardt, A. M., & Oster, J. L. (2024). A comparative study of cave system calcium isotope ratios: Implications for quantitative reconstruction of paleorainfall from speleothems. *Geochemistry, Geophysics, Geosystems*, *25*, e2024GC011691. https://doi.org/10.1029/2024GC011691

Received 30 MAY 2024
Accepted 12 SEP 2024

Abstract Variations in speleothem calcium isotope ratios ($\delta^{44}Ca$) are thought to be uniquely controlled by prior carbonate precipitation (PCP) above a drip site and, when calibrated with modern data, show promise as a semi-quantitative proxy for paleorainfall. However, few monitoring studies have focused on $\delta^{44}Ca$ in modern cave systems. We present a multi-year comparative study of $\delta^{44}Ca$, carbon isotopes ($\delta^{13}C$), and trace elemental ratios from cave drip waters, modern calcite, and host rocks from two cave systems in California—White Moon Cave (WMC) and Lake Shasta Caverns (LSC). Drip water and calcite $\delta^{44}Ca$ from both caves indicate PCP-driven enrichment, and we used a simple Rayleigh fractionation model to quantify PCP variability over the monitoring period. Modern calcite trace element and $\delta^{44}Ca$ data positively correlate at WMC, but not at LSC, indicating a shared PCP control on these proxies at WMC but not at LSC. At both WMC and LSC, we observe an inverse relationship between PCP and rainfall amounts, though this relationship is variable across individual drip sites. Our modeled data suggest that WMC experiences ~20% more PCP than LSC, consistent with the fact that WMC receives less annual rainfall. This work supports speleothem $\delta^{44}Ca$ as an independent constraint on PCP that can aid in the interpretation of other hydrologically sensitive proxies and provide quantitative estimates of paleorainfall. Additional, long-term monitoring studies from a variety of climate settings will be key for understanding $\delta^{44}Ca$ variability in cave systems more fully and better constraining the relationship between PCP and rainfall.

Plain Language Summary Chemical analyses on the minerals that make up stalagmites can provide useful information about how rainfall varied in the past, but most of the chemical parameters measured in stalagmites can respond to several complex environmental influences in addition to rainfall amount. Stalagmite calcium (Ca) isotope ratios can provide more direct information about past rainfall variability but haven't been closely studied in modern cave systems. In this study, we present new Ca isotope measurements of cave drip waters and modern calcite mineral samples collected at a seasonal-to-annual resolution from two sites in California that experience different amounts of yearly rainfall. We find that periods of less rainfall at each individual cave generally correspond to higher Ca isotope ratios and that the drier of the two caves experienced less water infiltration overall during the study period. These findings support the idea that Ca isotope ratios in cave systems are controlled by the amount of water infiltrating the cave and can be used in combination with other data from stalagmites to reconstruct rainfall variability in the past. This type of information about past rainfall patterns can help planners assess future water availability, which is especially important in drought-prone regions such as California.

1. Introduction

Carbonate speleothems have become valuable records of paleoclimate and paleoenvironmental change due to their precise absolute chronologies using U-Th dating techniques, their (semi-) continuous deposition, and their widespread global distribution (Wong & Breecker, 2015). To date, a wide variety of geochemical proxies have been applied in speleothem studies to reconstruct a multifaceted picture of past climate and environmental changes. The oxygen isotopic composition ($\delta^{18}O$) of speleothem carbonate records changes in meteoric water isotope ratios driven by shifts in precipitation amount, seasonality, and source; and measurements of speleothem $\delta^{18}O$ have been used to interpret hydroclimate response to climate changes on global, regional, and local scales (e.g., Cheng et al., 2016; Lachniet, 2009; Oster et al., 2020). Trace element ratios in speleothems (X/Ca) have

been shown to respond to local hydrologic changes via the influence of water infiltration rate and interaction with host rock on groundwater chemistry during flow from the surface to the cave (Fairchild & Treble, 2009) and have become widely applied as tracers of local effective precipitation rates (e.g., Serrato Marks et al., 2021; Xue et al., 2021). The carbon isotope ratios ($\delta^{13}C$) of speleothems are dependent on vegetation and soil characteristics of the surface above the cave site as well as hydrologic conditions during water flow through the host rock and have become an increasingly valuable proxy for paleo-environmental reconstruction (e.g., Fohlmeister et al., 2020).

While these geochemical measurements are useful paleoclimate proxies, especially when interpreted as complementary pieces of a multi-proxy approach, speleothem $\delta^{18}O$, trace element ratios, and $\delta^{13}C$ have traditionally been limited to qualitative interpretations of past climate changes due to the complex controls on these proxy systems. Recent efforts have aimed at developing quantitative records of precipitation using speleothem $\delta^{18}O$ (Hu et al., 2008; Medina-Elizalde et al., 2010; Wright et al., 2022) and trace element ratios (Warken et al., 2018). However, these approaches rely on ideal scenarios of clear-cut amount effect signal in rainfall $\delta^{18}O$ or speleothem records that overlap with modern observations, which are rare in speleothem-based climatological studies. In most cases, these proxies are influenced by multiple environmental factors that can be challenging to disentangle (e.g., Oster et al., 2021). Thus, the development of reliable quantitative rainfall proxies remains an important, yet elusive, goal in the field of speleothem paleoclimatology.

Calcium (Ca) is a common mobile metal that is cycled via various biogeochemical processes on Earth's surface. There are six stable isotopes of calcium (^{40}Ca, ^{42}Ca, ^{43}Ca, ^{44}Ca, ^{46}Ca, ^{48}Ca) that can be measured in organic and mineral phases to elucidate geochemical cycles at a wide range of spatial and temporal scales (Griffith et al., 2020). Despite its abundance in speleothem carbonate, calcium isotopic compositions ($\delta^{44}Ca$) have not been widely applied in speleothem studies. Recently, however, speleothem $\delta^{44}Ca$ has been proposed as a quantitative proxy for paleo-hydroclimate variability (Owen et al., 2016). Speleothem $\delta^{44}Ca$ is understood to be uniquely controlled by the degree of carbonate formation along the water flow path above a cave drip site (Figure 1), a process termed prior carbonate precipitation (PCP) that can be related to the amount and rate of water flow into the cave. Thus, if calibrated using observations of $\delta^{44}Ca$ response to rainfall variability in the modern environment, reconstructed PCP variability using speleothem $\delta^{44}Ca$ offers a potential method for quantitative interpretation of past rainfall rates (Owen et al., 2016).

Since there is no mass-dependent fractionation of Ca isotopes during carbonate dissolution, when acidic infiltrating water in the karst zone contacts cave host rock, it will take on the host rock $\delta^{44}Ca$ composition (Owen et al., 2016). When this Ca-enriched water comes into contact with air-filled void spaces above and within a cave that have lower atmospheric pCO_2 than the soil zone with which the water equilibrated, the water may degas CO_2, driving carbonate mineral precipitation. Since the lighter calcium isotope (^{40}Ca) preferentially enters the solid phase during carbonate precipitation (Gussone et al., 2005; Reynard et al., 2011; Tang et al., 2008), infiltrating waters will become enriched in the heavier Ca isotope (^{44}Ca) relative to the carbonate host rock as a function of the amount of PCP that occurs (de Wet et al., 2021; Li et al., 2018; Magiera et al., 2019; Owen et al., 2016). PCP is controlled by the amount of water infiltration, which is related to effective rainfall above the cave system, as well as the saturation state of infiltrating water, which depends on temperature and soil respiration rates (Stoll et al., 2012, 2023). Large amounts of rapidly infiltrating water caused by relatively higher local effective rainfall will fill void spaces in the karst zone, decreasing the residence time of the water and limiting the opportunity for degassing and PCP (Figure 1b) (de Wet et al., 2021; Fairchild & Treble, 2009; Owen et al., 2016; Sherwin & Baldini, 2011). Conversely, during periods of relative aridity and less water infiltration, void spaces in the karst zone are more air-filled and better ventilated, allowing more opportunity for degassing and PCP (Figure 1a). The fraction of the amount of Ca dissolved from the host rock that remains in solutions when infiltrating water reaches the cave can be quantified using transfer functions that describe the evolution of Ca isotopes during PCP as a Rayleigh fractionation process (de Wet et al., 2021; Owen et al., 2016). Rainfall and temperature changes can also influence PCP by shifting vegetation and/or soil respiration regimes, which change the saturation state of infiltrating water. For example, decreased rainfall amounts can decrease vegetation density and soil pCO_2, which decreases the saturation state of the cave drip water, attenuating PCP even as the lessened water infiltration rate enhances it (Lechleitner et al., 2021).

Owen et al. (2016) first related speleothem $\delta^{44}Ca$ to specific effective rainfall rates using $\delta^{44}Ca$ and rainfall measurements from the modern cave system and estimated the degree of aridification at Heshang Cave in central

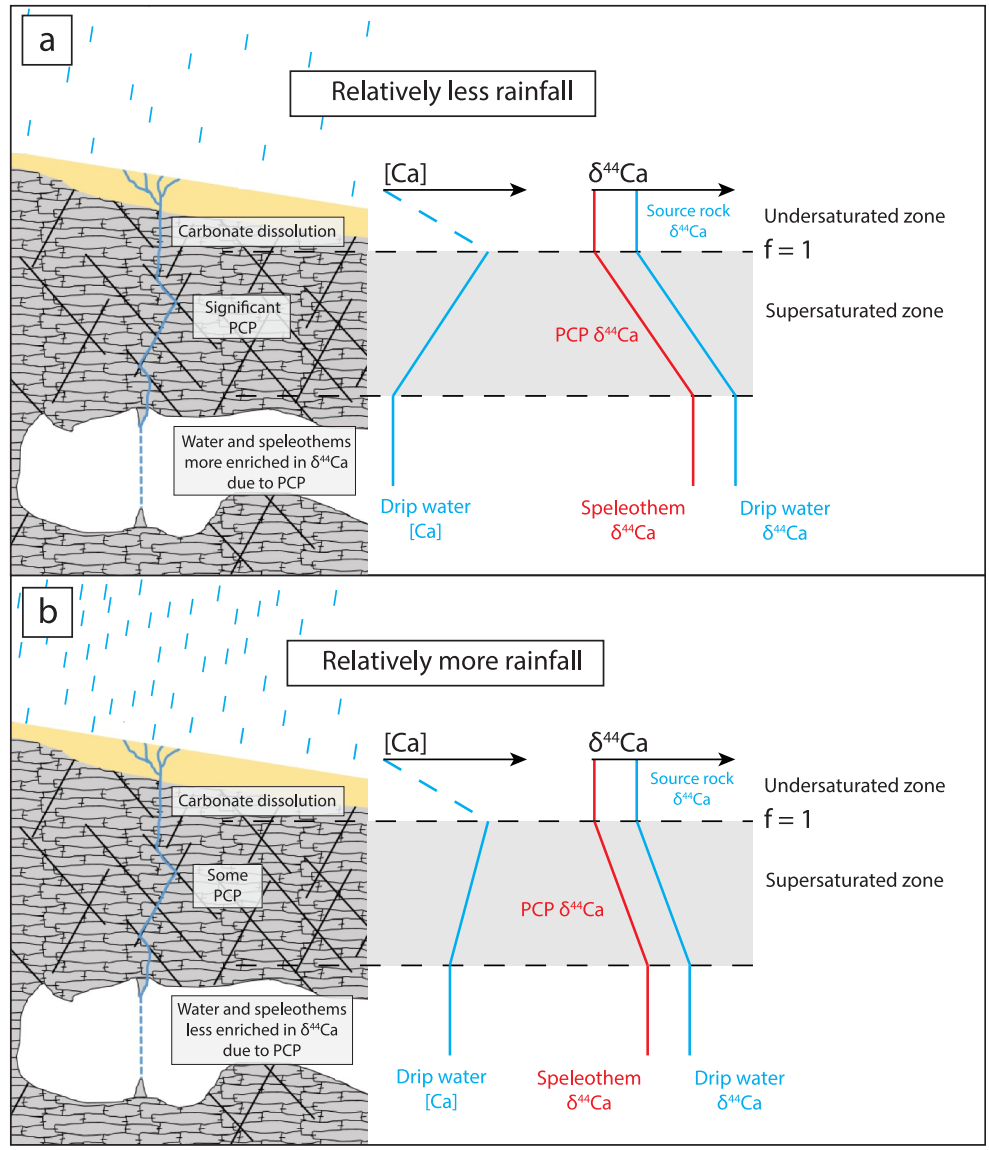

Figure 1. Illustration of seepage water flow and [Ca] and $\delta^{44}Ca$ evolution under relatively drier (a) and relatively wetter conditions (b). Adapted from Owen et al. (2016).

China in response to the 8.2 Kyr event. Li et al. (2018) further developed the proxy by analyzing the $\delta^{44}Ca$ variability within the portion of the same Heshang Cave stalagmite that grew during the 20th century and comparing that record to observed rainfall rates. The authors found that the nearly annually resolved speleothem $\delta^{44}Ca$ correlated significantly with both observed precipitation and the dryness/wetness index from the nearby Yangtze River, substantiating the reliability of the speleothem $\delta^{44}Ca$ rainfall proxy. Since then, measurements of speleothem $\delta^{44}Ca$ have been used as part of a multi-proxy approach to demonstrate a large increase in PCP during the transition from Marine Isotope Stage 5e to the Late Eemian Arid Period in Mawmluh Cave, India (Magiera et al., 2019), as well as to characterize drought dynamics during the 4.2 Kyr event in Dharamjali Cave, India (Giesche et al., 2023). Additionally, de Wet et al. (2021) use speleothem $\delta^{44}Ca$ to generate semi-quantitative estimates of rainfall variability during the 8.2 Kyr event in coastal California and directly compare the wet and dry extremes of the early and middle Holocene with modern "climate whiplash." The $\delta^{44}Ca$ proxy has also been utilized to constrain the influence of PCP and distinguish vegetation and soil components of speleothem $\delta^{13}C$ (Lechleitner et al., 2021; Stoll et al., 2023).

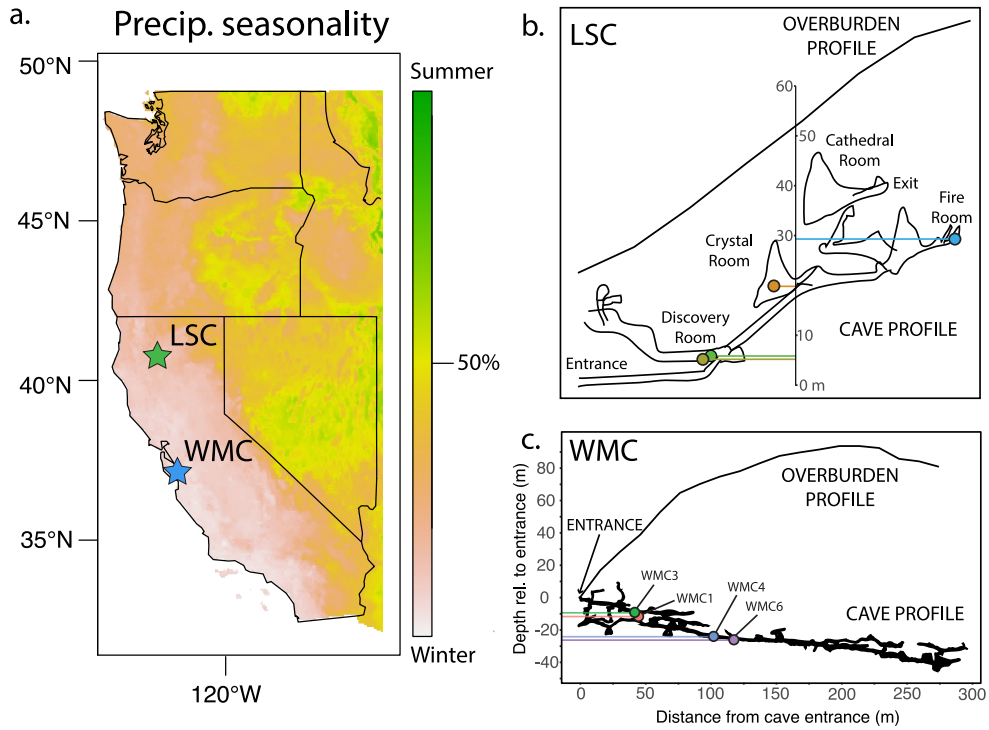

Figure 2. (a) Locations of WMC and LSC study sites with precipitation seasonality of region (30-year normal (1991–2020) from PRISM Climate Group (2021)). WMC = White Moon Cave: blue star; LSC = Lake Shasta Caverns: green star. (b) LSC profile with locations and depths of monitoring sites. Map is based on unpublished survey data provided by D. Mundt. (c) WMC profile with locations and depths of monitoring sites.

Despite this recent work, few studies have rigorously tested the assumptions of the δ^{44}Ca proxy in modern cave settings using modern calcite and drip water. Non-climate factors, such as cave system geology, flow path geometry, and host rock variability, may also impact Ca isotopic cycling across an individual cave system but have not been fully explored. The spatial and temporal variability of the Ca isotopic fractionation factor between drip waters and precipitated carbonate mineral phases within cave systems are also not well constrained, despite the observation that PCP reconstructed from fossil speleothem records are sensitive to the fractionation factor measured from the modern system that is used for the calculations (de Wet et al., 2021; Stoll et al., 2023).

In this study, we present coeval measurements of δ^{44}Ca, δ^{13}C, and trace element to calcium ratios (Mg/Ca, Sr/Ca, Ba/Ca) from drip waters, modern calcite grown on glass plates installed under drip sites, and carbonate host rocks from two cave systems in the western United States (US)—White Moon Cave (WMC) in coastal California and Lake Shasta Caverns (LSC) in northern California (Figure 2). These cave systems span climatological and geologic gradients and represent valuable natural laboratories in which to test the Rayleigh fractionation model framework at multiple drip sites within each cave system. The δ^{44}Ca data is compared with coeval δ^{13}C and trace element ratios to test the degree to which this newly developing proxy system provides complementary data to these more established, but complex, proxies for water infiltration and PCP. We test the sensitivity of calculated PCP amounts to measured variability in the δ^{44}Ca composition of the cave host rock, which is assumed to be the Ca isotope source for drip waters and calcite in the cave, and to the fractionation factor determined between drip water and precipitating calcite. Finally, we compare PCP reconstructed from modern calcite δ^{44}Ca data with the amount of rainfall that occurred during the interval of calcite growth to assess the degree to which the PCP amounts reconstructed from δ^{44}Ca align with measured rainfall variability.

1.1. Site Description—White Moon Cave

White Moon Cave (WMC) was formed in the late Paleozoic San Vicente marble in the Santa Cruz Mountains east of Davenport, CA (37.02°N, 122.18°W, 167 m asl). The marble host rock is intruded by Cretaceous quartz diorite and overlain by Miocene sandstones and shales and contains variable amounts of accessory mica phases (Hart &

Williams, 1978). The modern cave entrance lies within a twentieth-century quarry that transects the natural cave system. Cave air pCO_2 measured in winters and summers between 2018 and 2022 ranges from 479 to 726 ppm (mean: 603 ± 81 ppm, $n = 9$ across four locations) typically with slightly lower values closer to the cave entrance (Table S1 in Supporting Information S1). We analyzed samples from four sites that span the vertical depth of the cave. Sampling sites WMC1 and WMC3 are within the upper portion of the cave, approximately 10 m below the modern entrance and approximately 45 m below the surface. Sites WMC4 and WMC6 are deeper, approximately 25 m below the modern entrance and approximately 95 m below the surface (Figure 2c). The cave floor is composed of exposed marble and silicate and mica-rich sand with pebbles and cobbles that evince significant downward water flow through the cave during high rainfall events.

White Moon Cave experiences a Mediterranean climate with warm, dry summers and cool, wet winters. Seasonal temperature variation is small and moderated by the cave's coastal location (11.3–18.0°C; Arguez et al., 2010). The region receives ~759 mm/yr of precipitation on average (1950–2016), >80% of which occurs during the cool season (October–March; US Climate Data; Figure 2a). Precipitation is primarily sourced from winter storms that originate in the northern or midlatitude Pacific Ocean. However, the region also receives precipitation from atmospheric rivers and narrow streams of near-surface water vapor associated with extratropical cyclones that source moisture from the central or eastern tropical Pacific, which can cause extreme flooding in California (Dettinger, 2011).

1.2. Site Description—Lake Shasta Caverns

Lake Shasta Caverns (LSC) is a commercial cave located on the eastern side of the McCloud arm of Shasta Lake (40.8°N, 122.3°W, 725 m asl), approximately 32 km north of Redding, CA. The cave formed in the McCloud Limestone which is early Permian in age and consists of calcarenite with varying amounts of crinoid, bryozoan, and fusulinid foraminifera fossils (Demirmen & Harbaugh, 1965). The cave is accessed via two artificial entrances (marked "Entrance" and "Exit" in Figure 2b). The only known natural entrance is located approximately 30 m above the Cathedral Room (Figure 2b). Cave air pCO_2 measured in winters and summer between 2018 and 2022 ranges from 470 to 904 ppm (mean: 665 ± 107 ppm, $n = 16$ across 5 locations) typically with lower values closer to the entrance and exit (i.e., in the Discovery Room and Cathedral Room) (Table S1 in Supporting Information S1). The presence of tour groups likely obfuscates any natural ventilation pattern that would otherwise be driven by seasonal temperature variations. Five sampling sites were chosen for drip water and modern calcite analyses based on the availability of water and in the interest of spanning the vertical extent of the cave. Due to the surface topography, the Fire Room is the deepest LSC site sampled at ~40 m beneath the surface. Site Discovery Rooms A, B, and C are located close to each other in the same room approximately 30 m beneath the surface. The Crystal Room sampling site is also ~30 m beneath the surface (Figure 2b).

The region is characterized by cool, wet winters and hot, dry summers. Redding, CA, approximately 15 km south of LSC, receives an average of 879 mm/yr of precipitation (1981–2010), approximately 90% of which occurs between October and March (Figure 2a). Like WMCs, LSCs are affected by atmospheric river storms that can deliver significant amounts of precipitation over relatively short intervals (days to weeks).

2. Materials and Methods

2.1. Cave Monitoring

Drip water and modern calcite samples were analyzed for $\delta^{44}Ca$, $\delta^{13}C$, and trace element concentrations (Mg, Sr, and Ba) and host rock samples were analyzed for $\delta^{44}Ca$. Water samples were collected instantaneously at each drip site during sampling trips and were filtered through 0.2-micron sterile syringe filters into 50 mL LDPE vials and immediately split for each analysis type. At slower drip sites, LDPE bottles were left under the drip at the beginning of the sampling trip and collected on the return trip out of the cave. No bottle was left for more than 2 hr, and no calcite precipitate was ever observed within a collection bottle. For $\delta^{13}C$ analysis, 2 ml of water was injected into helium-flushed 12 ml rubber-capped Labco Exetainer vials containing 1 ml phosphoric acid in the cave immediately after filtering. For $\delta^{44}Ca$ and trace element analysis, the original sample vial was acidified with concentrated trace metal grade HNO_3 to a final concentration of ~3% HNO_3 within 48 hr of collection. All water samples were kept refrigerated with minimal head space until analysis. Due to slow drip rates, sufficient water for all analyses could not be collected during some sampling trips, especially during summers when drip rates are

low. The installation and collection dates of all glass plates and collection dates for all drip waters are listed in Table S2 of the Supporting Information S1.

Glass plates were etched using a polishing wheel and installed underneath drip sites to provide an artificial substrate for the precipitation of modern calcite. After collection, all the precipitated calcite was scraped off the plates with a clean scalpel and homogenized prior to splitting for analysis. It was not possible to analyze $\delta^{44}Ca$, $\delta^{13}C$, and trace element concentrations for every sample due to insufficient sample size. Representative host rock samples were collected from the surface and within each cave and powders were drilled from fresh surfaces for $\delta^{44}Ca$ analysis.

Drip waters and modern calcite samples were collected from four drip sites at WMC during summer and winter caving trips. Seven waters and six and four modern calcite samples were collected from WMC1 and WMC3 respectively between March 2017 and December 2022. Five waters and four modern calcite samples were collected from WMC4 and WMC6 between February 2019 and December 2022. Three samples of the marble host rock were collected from the surface near the cave entrance and one sample was collected from within the WMC.

Drip waters were collected from five drip sites and modern calcite samples from three drip sites at LSC during summer and winter caving trips. Four drip water samples were collected from sites Discovery Room B and Crystal Room between June 2018 and December 2022, but glass plates for modern calcite could not be installed at these sites because of the topography of the cave floor and proximity to the tour path. Drip water and modern calcite samples were collected from sites Discovery Room A, Discovery Room C, and Fire Room between February 2019 and December 2022. Two samples of the limestone host rock were collected from the surface above LSC and two were collected inside the cave in the Crystal Room and near the cave exit.

2.2. Trace Element, Calcium and Carbon Isotopic Analyses

For the measurement of trace element concentrations, between 0.2 and 3 mg of powder were split from the modern calcite samples depending on how much calcite had been collected from the glass plate. Powder samples were dissolved in concentrated trace metal grade HNO_3 and diluted to a concentration of 3% HNO_3. Drip water and dissolved calcite samples were analyzed using a Thermo Finnigan iCapQ ICP-MS in solution mode at Vanderbilt University (VU). Calibration standards were prepared using a custom mixed solution from Inorganic Ventures (Christiansburg, VA) containing Na, Ca, and Mg for high-concentration elements and the IV-71A standard solution for low-concentration elements. These standard solutions were mixed online with an internal standard solution (IV-71D) and were also run as unknowns. The standard solution IV-Stock-10 was also run as an unknown during each analysis period. Each batch of water and dissolved calcite samples was run in two separate analyses, first for low-concentration elements (Sr, Ba) and then for high-concentration elements (Ca, Mg).

For $\delta^{13}C$ analysis, approximately 0.20 mg of powder was split from the modern calcite and host rock samples, added to LabCo exetainer vials, and dried overnight at 50°C. Vials were then flushed with He for 10 min. Anhydrous orthophosphoric acid (<0.1 mL) was added to the vials and the samples were allowed to react for at least 1 hr at 70°C. Evolved CO_2 from drip water and dissolved calcite samples were then run on a ThermoFisher Scientific Delta V Isotope Ratio Mass Spectrometer (IRMS) equipped with a GasBench-II at VU. Samples were analyzed with the ThermoCalcite and VU Coral in-house carbonate standards, both of which are referenced to the IAEA603 and NBS-19 standards. Two additional in-house standards, VU Marble and Pol2, are also run as unknowns in each run. Corrections were conducted using the USGS LIMS for Light Stable Isotopes data reduction scheme (Coplen, 1998). The long-term uncertainty for $\delta^{13}C$ is ±0.07‰ (1σ) based on repeat measurements of VU Marble. Final $\delta^{13}C$ values are presented in per-mil (‰) relative to the international standard V-PDB (Vienna PeeDee Belemnite).

WMC carbonate and water samples collected before 2020 ($n = 25$) were first reported by de Wet et al. (2021). WMC samples collected after the beginning of 2020 ($n = 18$) and all LSC samples ($n = 31$) were prepared for $\delta^{44}Ca$ analysis at VU and analyzed on a ThermoFisher Scientific Triton Plus Thermal Ionization Mass Spectrometer (TIMS) at The Ohio State University (OSU). Splits were taken from drip water samples and dried down to isolate 7 μg of Ca based on measured Ca concentrations. For the modern calcite and host rock samples, 17.5 μg of powder was used. The dried-down water samples and carbonate powder samples were dissolved in 200 μL concentrated OPTIMA HCl, spiked with 60 μL ^{43}Ca-^{42}Ca double-spike (Wogsland, 2020) to achieve the target spike-to-sample ratio of 0.428 following Lehn et al. (2013) and sonicated for 10 min to ensure complete mixing.

Spiked samples were dried down and redissolved in 75 μL 1.5M OPTIMA-grade HCl in preparation for purification using cation exchange columns. Subtraction of the double-spike component from the sample mixture is done offline after analysis using an iterative mathematical routine. The use of the double-spike allows for the measurement to be corrected for the mass-dependent fractionation that occurs during sample preparation and analysis.

Samples were processed through an ion exchange column procedure calibrated at VU using 1 mL MCI Gel CK08P resin to separate Ca ions (Griffith et al., 2008; Wogsland, 2020). The resin was cleaned prior to use with multiple rinses of 8M OPTIMA-grade or distilled HCl and ultra-pure Milli-Q water and conditioned with water until the pH was ∼5.5. Columns filled with resin were washed with 3 mL 6M OPTIMA-grade HCl, then 3 mL ultra-pure Milli-Q water, and were then conditioned with 3 mL 1.5M OPTIMA-grade HCl. The samples were then pipetted directly onto the conditioned columns and the sample vials were rinsed twice with 250 μL 1.5M OPTIMA-grade HCl, which was also pipetted onto the columns. The columns were rinsed with 6.5 mL 1.5M OPTIMA-grade HCl and then the Ca fraction was collected using a rinse of 4.5 mL 1.5M OPTIMA-grade HCl. To minimize any organics after columns, 0.5 mL of H_2O_2 was added to each sample and refluxed on a hotplate set to 95°C for ∼8 hr and then dried down.

For the analyses on the TIMS at OSU, samples were dissolved in 2 μL 1.5 or 1.8N distilled HCl and 1 μL splits were loaded onto outgassed tantalum single filaments manufactured in house. After the sample split dried down completely 1.25 μL of 3.2N ultrapure phosphoric acid was loaded onto the filament (Fantle & DePaolo, 2005) and dried down for 10 min. The filaments were then heated slowly to 1.2 A and held for 1 min. The current was increased slowly until the filaments glowed red (∼2.4 A) at which point the current was immediately shut off. Sixteen samples were analyzed per run along with three analyses of NIST SRM 915a and two analyses of NIST SRM 915b using an automated filament heating and analysis procedure. Data are presented in δ^{44}Ca notation (Equation 1) relative to bulk silicate earth (BSE) following Heuser et al. (2016). The average external 2σ over the analysis period at OSU on NIST SRM 915a was 0.07‰ (2σ, n = 33). Analysis of NIST SRM 915b at OSU yielded a value of δ^{44}Ca = −0.30 ± 0.10‰ (2σ, n = 23) in agreement with previously reported values (−0.29‰ from Heuser et al. (2016)) and uncertainty reported over the analysis period at Cambridge University (de Wet et al., 2021).

$$\delta^{44}\mathrm{Ca} = \left(\frac{\left(\frac{[44\mathrm{Ca}]}{[40\mathrm{Ca}]}\right)\mathrm{Sample}}{\left(\frac{[44\mathrm{Ca}]}{[40\mathrm{Ca}]}\right)\mathrm{Standard}} - 1 \right) * 1000 \quad (1)$$

2.3. Rainfall Data

Daily rainfall data for WMC were acquired from the University of California Integrated Pest Management (UC IPM) De Laveaga weather station in Santa Cruz, CA (37.0°N, 122.0°W; elev: 91 ft asl; https://ipm.ucanr.edu/calludt.cgi/WXDESCRIPTION?MAP=&STN=SNTACRUZ.A). The De Laveaga UC IPM station is approximately 17.5 km east of Davenport, CA, which is near WMC. Daily rainfall for LSC was acquired from the Whiskeytown UC IPM station in the Whiskeytown-Shasta-Trinity National Recreation Area, CA (40.62°N, 122.53°W; elev. 2,195 ft asl; https://ipm.ucanr.edu/calludt.cgi/WXDESCRIPTION?MAP=&STN=-WHISKTWN.C). The station is approximately 20 km southwest of LSC.

3. Results

3.1. White Moon Cave

White Moon Cave drip water δ^{44}Ca measurements range from −0.42‰ to −0.14‰ (relative to BSE) with a mean of −0.26‰ (2σ = 0.12, n = 22) (Figure 3, Figure S1a in Supporting Information S1; Table S2). This range is about 3x the uncertainty for the analysis of the Ca isotopic standards. Qualitatively, the drip water from the shallower sites WMC1 (mean = −0.29‰, 2σ = 0.15, n = 7) and WMC3 (mean = −0.29‰, 2σ = 0.10, n = 7) tend to display more negative δ^{44}Ca values than the deeper sites WMC4 (mean = −0.25‰, 2σ = 0.07, n = 5) and WMC6 (mean = −0.21‰, 2σ = 0.10, n = 3) (T Test p value = 0.118) (Figure S1a in Supporting Information S1). Based on drip water samples collected during summer (mean = −0.29‰, 2σ = 0.13, n = 6) and winter

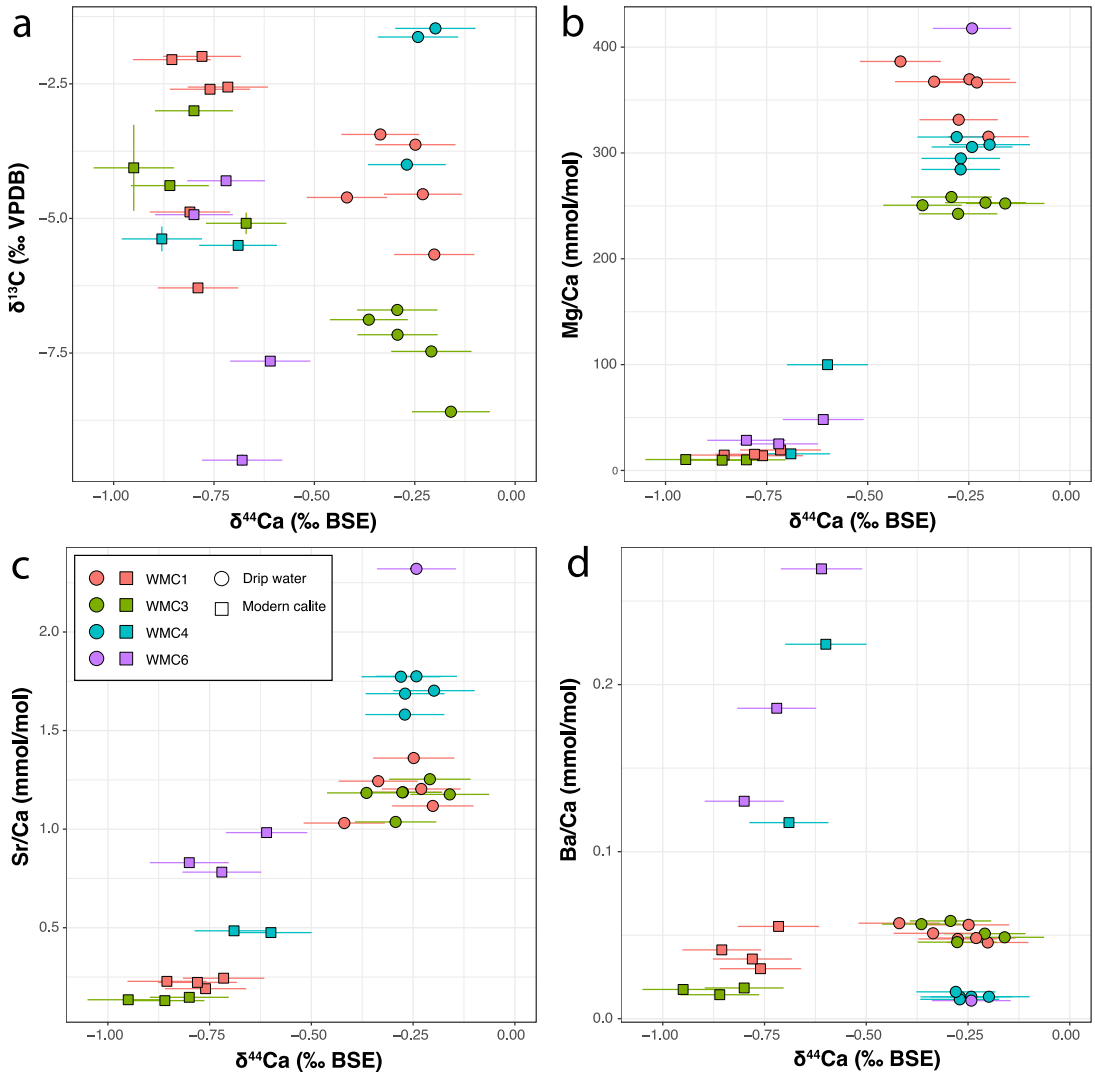

Figure 3. Cross plots of WMC drip water and modern calcite $\delta^{44}Ca$ versus $\delta^{13}C$ (a), Mg/Ca (b), Sr/Ca (c), and Ba/Ca (d). Error bars for $\delta^{44}Ca$ show the average external 2σ over the analysis period on NIST SRM 915a (0.1‰). Error bars for $\delta^{13}C$ show the 2σ for each individual measurement. The analytical uncertainty for the trace element data is smaller than the symbols.

(mean = −0.26‰, $2\sigma = 0.12$, $n = 13$) sampling trips, there is not a seasonal signal despite the extreme winter bias in rainfall at the site (Figure 4).

White Moon Cave marble host rock $\delta^{44}Ca$ measurements are lower than the drip waters, except for one sample. They range from −0.59‰ to −0.27‰ BSE (mean = −0.45‰, $2\sigma = 0.26$, $n = 4$) with samples that have the highest proportion of accessory mica minerals displaying the lowest $\delta^{44}Ca$ (Figure S1a in Supporting Information S1; Table S2). All measured $\delta^{44}Ca$ drip water values are less negative than the mean (and the median) host rock $\delta^{44}Ca$, though the least negative individual host rock measurement of −0.26‰ BSE is less negative than 13 of the 20 total WMC drip water samples analyzed (Figure S1a in Supporting Information S1).

White Moon Cave drip water $\delta^{13}C$ values range from −8.59‰ to −1.47‰ VPDB with a mean of −5.01‰ ($2\sigma = 4.32$, $n = 15$) (Figure 3a, Figure S1b in Supporting Information S1; Table S2). Due to slow drip rates, it was not possible to collect enough water to analyze $\delta^{13}C$ from all four drip sites during every sampling trip. The shallower sites WMC1 (mean = −4.38‰, $2\sigma = 1.70$, $n = 5$) and WMC3 (mean = −7.36‰, $2\sigma = 1.49$, $n = 5$) tend to display more negative $\delta^{13}C$ values than the deeper sites, WMC4 (mean = −2.37‰, $2\sigma = 2.83$, $n = 3$) and

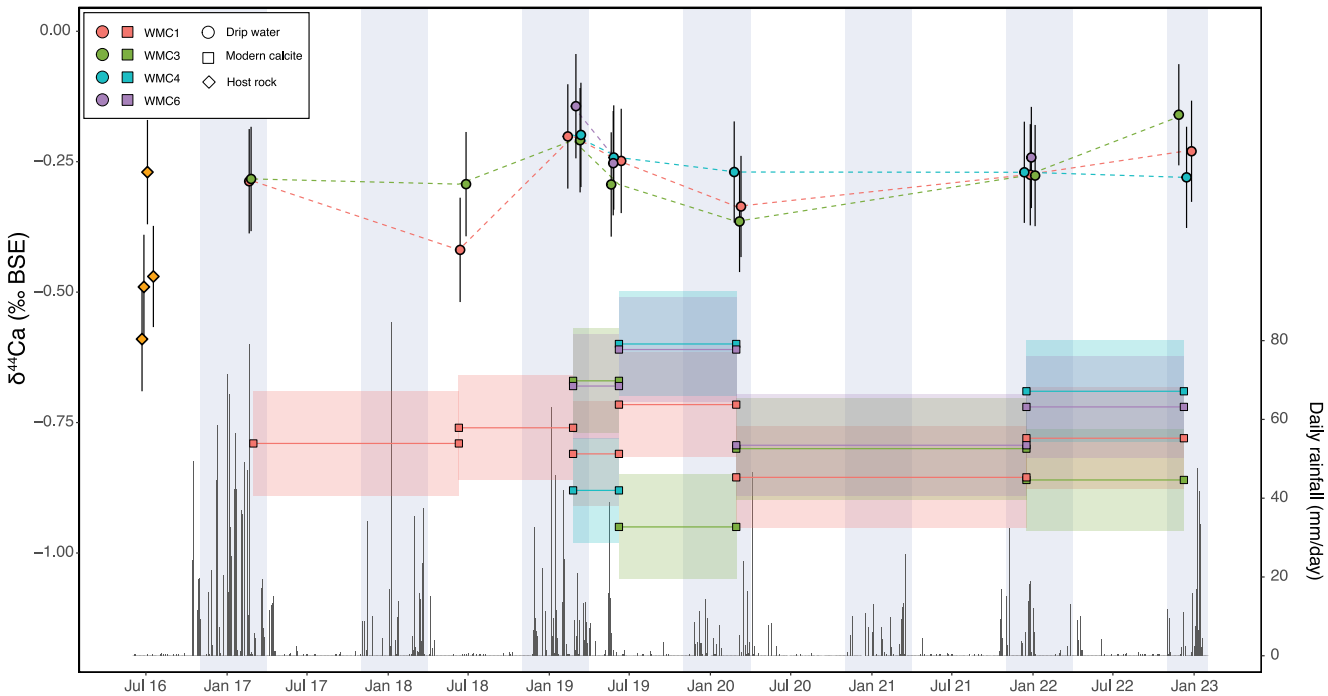

Figure 4. WMC host rock, drip water, and modern calcite $\delta^{44}Ca$ data and daily rainfall totals from the De Laveaga UC IPM station. Note that the modern calcite $\delta^{44}Ca$ values are the same for the WMC3 and WMC6 modern calcite samples that precipitated in the cave from February 2020 to January 2022. In the plot, the WMC6 data points are shifted upward by ∼0.01‰ for the purpose of legibility. Error bars for host rock and drip water data and colored shading for modern calcite data show the average external 2σ over the analysis period on NIST SRM 915a (0.1‰). Vertical shading denotes the core of the wet season at the WMC (November–March).

WMC6, though there is only one measurement from WMC6 (−4.29‰ collected on 2/29/20) (T Test p value = 0.016). As with $\delta^{44}Ca$, there is not a clear seasonal signal in the WMC drip water $\delta^{13}C$ data.

White Moon Cave drip water Mg/Ca ranges from 242.49 to 417.68 mmol/mol with a mean for all drip sites of 312.88 mmol/mol (2σ = 107.35, n = 17) (Figure 3b, Figure S1c in Supporting Information S1; Table S2). Site WMC1 displays the highest Mg/Ca, except the one measurement from WMC6 in December 2021, as well as the largest range of variability with a maximum of 386.46 mmol/mol in June 2018 and a minimum of 315.36 mmol/mol in February 2019. Drip water Mg/Ca from shallower WMC sites do not display a difference relative to deeper sites, nor is there a clear difference between summer (mean = 330.02 mmol/mol, 2σ = 118.21, n = 4) and winter (mean = 307.61 mmol/mol, 2σ = 106.58, n = 13).

White Moon Cave drip water Sr/Ca measurements range from 1.03 to 2.32 mmol/mol (mean = 1.40 mmol/mol, 2σ = 0.7, n = 17) across all drip sites with the deeper WMC4 and WMC6 sites displaying higher values than the shallower WMC1 and WCM3 sites (T Test p value = 0.002) (Figure 3c, Figure S1e in Supporting Information S1; Table S2). There is not a clear difference between summer and winter drip water Sr/Ca.

White Moon Cave drip water Ba/Ca values range from 0.01 to 0.06 mmol/mol (mean = 0.04 Ba/Ca, 2σ = 0.04, n = 17) (Figure 3d, Figure S1g in Supporting Information S1; Table S2). Sites WMC1 and WMC3 display significantly higher Ba/Ca values than the deeper WMC4 and WMC6 sites (T Test p value < 0.001). As with Mg/Ca and Sr/Ca (and $\delta^{44}Ca$ and $\delta^{13}C$), there is not a clear difference between summer and winter.

Modern calcite $\delta^{44}Ca$ values from White Moon Cave range from −0.95‰ to −0.60‰ BSE (mean = −0.76‰, 2σ = 0.19, n = 17) (Figure 3, Figure S1a in Supporting Information S1; Table S2). This range of values is more than 3x the uncertainty for the analysis of the Ca isotopic standards. White Moon Cave modern calcite values are offset from drip water $\delta^{44}Ca$ values by −0.81‰ to −0.19‰, following the expectation that the lighter ^{40}Ca isotope preferentially enters the solid phase during carbonate precipitation (Reynard et al., 2011). Plate calcites from the shallower WMC1 and WMC3 sites tended to display more negative $\delta^{44}Ca$ relative to calcite from the deeper WMC4 and WMC6 sites (T Test p value = 0.08) (Figure S1a in Supporting Information S1).

Using the mean of the drip water and modern calcite values, we measure a Ca isotopic fractionation between calcite and water (Δ^{44}Ca) of −0.50‰ at WMC1, which corresponds to an α value of 0.9995. At WMC3 the measured Δ^{44}Ca is −0.55‰ and α is 0.9994. At WMC4 Δ^{44}Ca is −0.47‰ and α is 0.9995. And WMC6 Δ^{44}Ca is −0.49‰ and α is 0.9995. The mean Δ^{44}Ca during the monitoring period across all WMC sites is −0.50‰ and α is 0.9995 (Table S3 in Supporting Information S1). These fractionation factors are similar to but slightly higher than those based on monitoring data from Heshang Cave (α = 0.9987; Owen et al., 2016) and Mawmluh Cave (0.99929; Magiera et al., 2019) and previously for WMC4 (α = 0.9993) and WMC6 (0.9995) in de Wet et al. (2021).

Measurements of δ^{13}C from WMC modern calcite samples collected between June 2018 and December 2022 ranged from −9.49‰ to −1.99‰ VPDB with a mean of −4.64‰ (2σ = 4.08, n = 16) (Figure 3a, Figure S1b in Supporting Information S1; Table S2). The shallower WMC1 and WMC3 sites displayed less negative δ^{13}C relative to the deeper WMC4 and WMC6 sites (T Test p value = 0.03).

White Moon Cave modern calcite Mg/Ca values range from 9.71 to 99.95 mmol/mol (mean = 26.84 mmol/mol, 2σ = 49.72, n = 13), Sr/Ca values range from 0.13 to 0.98 mmol/mol (mean = 0.43 mmol/mol, 2σ = 0.61, n = 13), and Ba/Ca values from 0.01 to 0.27 mmol/mol (mean = 0.10 mmol/mol, 2σ = 0.18, n = 13) (Figures 3b and 3d, Figures S1d, S1f, and S1h in Supporting Information S1; Table S2). The deeper WMC4 and WMC6 sites display a larger range of variability in and generally higher values of modern calcite Mg/Ca (T Test p value = 0.06), Sr/Ca (T Test p value = 0.001), and Ba/Ca (T Test p value = <0.001) relative to the shallower WMC1 and WMC3 sites. Using mean WMC1 drip water and mean modern calcite trace element measurements, we calculated an Mg/Ca partition coefficient (Kd_{Mg}) of 0.04, Kd_{Sr} of 0.19, and Kd_{Ba} of 0.79. At WMC3, Kd_{Mg} is 0.04, Kd_{Sr} is 0.12, and Kd_{Ba} is 0.32. At WMC4, Kd_{Mg} is 0.17, Kd_{Sr} is 0.33, and Kd_{Ba} is 13.88. At WMC6, Kd_{Mg} is 0.08, Kd_{Sr} is 0.37, and Kd_{Ba} is 18.01 (Table S3 in Supporting Information S1).

3.2. Lake Shasta Caverns

Drip water δ^{44}Ca values from LSC range from −0.41‰ to −0.18‰ BSE (mean = −0.30‰, 2σ = 0.11, n = 17) (Figure 5, Figure S2a in Supporting Information S1; Table S2). Crystal Room tended to display the most negative drip water δ^{44}Ca values (mean = −0.36‰, 2σ = 0.10, n = 3) and Discovery Room A the least (mean = −0.26‰, 2σ = 0.12, n = 4) (T Test p value = 0.07). The other sites fall between Crystal Room and Discovery Room A (Discovery Room B: mean = −0.32‰, 2σ = 0.07, n = 4; Discovery Room C: mean = −0.30‰, 2σ = 0.12, n = 3; Fire Room: mean = −0.29‰, 2σ = 0.06, n = 4). The mean of the drip waters collected during the summer from the Discovery Room (mean = −0.26‰, 2σ = 0.14, n = 3) is less negative than that of winter drip samples (mean = −0.30‰, 2σ = 0.08, n = 11) and the least negative drip water δ^{44}Ca value was collected in the summer from Discovery Room A (−0.18‰ in June 2019), which may point to more PCP during the dry season (Figure 6). However, it was often not possible to collect drip water during the summer because LSC drip rates tend to be close to 0 during the summer months. For this reason, we are unable to fully investigate seasonal variability at LSC with the current drip water data set.

LSC host rock δ^{44}Ca values range from −0.41‰ to −0.31‰ BSE (mean = −0.36‰, 2σ = 0.12, n = 4) with two of the LSC host rock samples giving indistinguishable δ^{44}Ca values of −0.41‰. One LSC drip water δ^{44}Ca value from the Crystal Room site (−0.41‰ on 6/7/19) is more negative than the mean of the LSC limestone host rock δ^{44}Ca and indistinguishable from that of the two lowest host rock δ^{44}Ca values (Figure S2a in Supporting Information S1; Table S2).

LSC drip water δ^{13}C values range from −11.26‰ to −3.66‰ VPDB (mean = −9.38‰, 2σ = 0.42, n = 16). Discovery Room A displays the highest values and largest range of variability (mean = −6.80‰, 2σ = 6.13, n = 4). Drip water δ^{13}C values from the other sites tend to be more negative and much less variable (Discovery Room B: mean = −9.96‰, 2σ = 1.89, n = 4; Discovery Room C: mean = −10.48‰, 2σ = 0.11, n = 2; Fire Room: −10.46‰, 2σ = 0.69, n = 3; Crystal Room: −10.21‰, 2σ = 0.33, n = 3) (Figure 5a, Figure S2b in Supporting Information S1; Table S2).

LSC drip water Mg/Ca measurements range from 15.01 to 76.99 mmol/mol with a mean of all drip sites of 39.87 mmol/mol (2σ = 37.53, n = 17). Sr/Ca measurements range from 0.20 to 0.43 mmol/mol with a mean of all drip sites of 0.27 mmol/mol (2σ = 0.13, n = 17). Ba/Ca measurements range from 0.03 to 0.56 mmol/mol with a

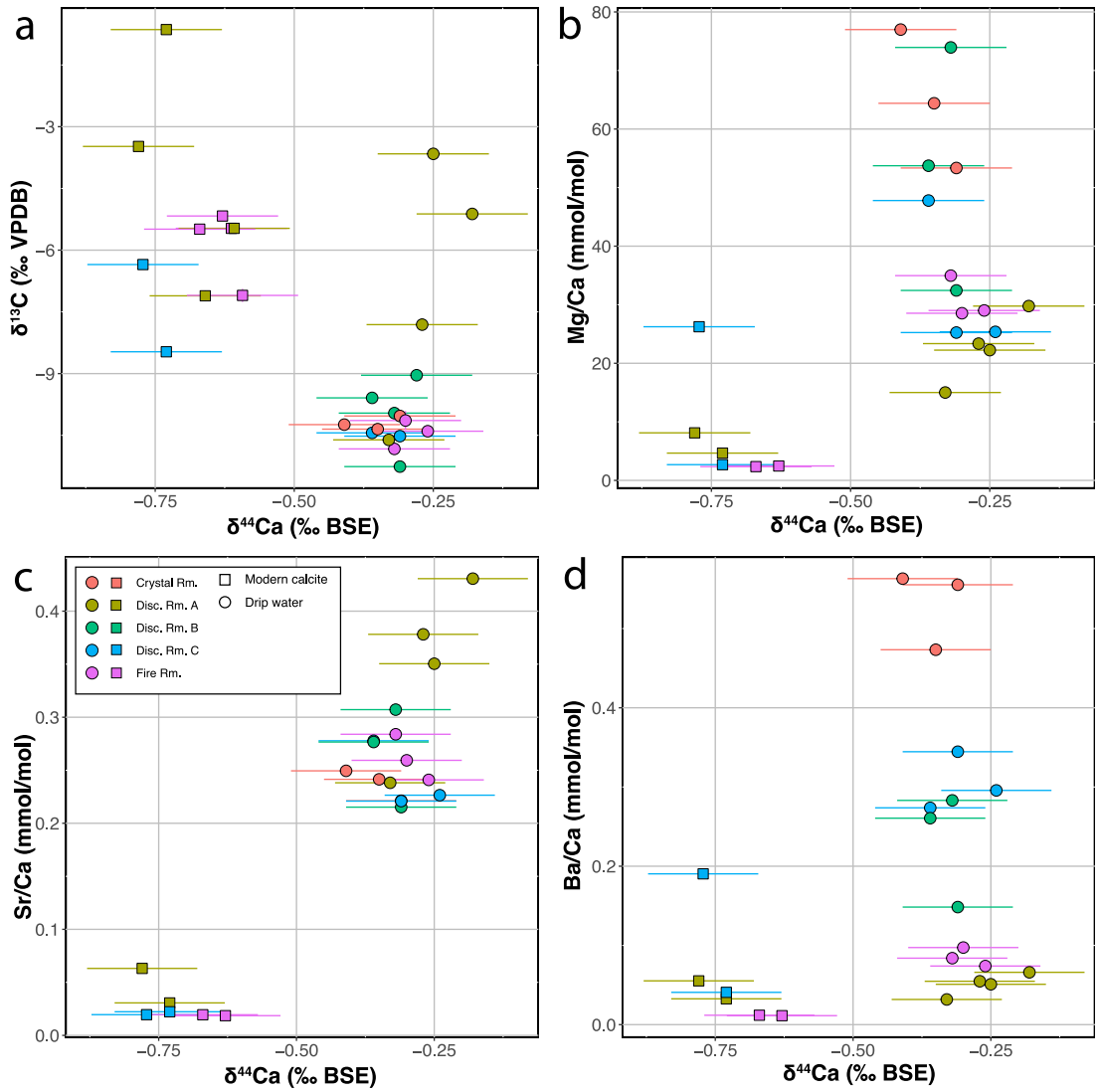

Figure 5. Cross plots of LSC drip water and modern calcite $\delta^{44}Ca$ versus $\delta^{13}C$ (a), Mg/Ca (b), Sr/Ca (c), and Ba/Ca (d). Error bars for $\delta^{44}Ca$ show the average external 2σ over the analysis period on NIST SRM 915a (0.1‰). Error bars for $\delta^{13}C$ show the 2σ for each individual measurement. The analytical uncertainty for the trace element data is smaller than the symbols.

mean of all drip sites of 0.24 mmol/mol (2σ = 0.36, n = 18) (Figures 5b–5d, Figures S2c, S2e, and S2g in Supporting Information S1; Table S2).

Measurements of $\delta^{44}Ca$ from Discovery Room A, Discovery Room C, and Fire Room modern calcite samples ranged from −0.78‰ to −0.59‰ BSE (mean = −0.68‰, 2σ = 0.14, n = 10). This range of values is roughly 2x the uncertainty for the analysis of the Ca isotopic standards. Mean LSC modern calcite values are offset from mean drip water $\delta^{44}Ca$ values by an average of −0.5‰ (Figure 5a). Fire Room modern calcite values tend to be higher than Discovery Room C and slightly higher than Discovery Room A, both of which are shallower than Fire Room relative to the surface above the cave (T Test p value = 0.08) (Figure 5a, Figure S2a in Supporting Information S1; Table S2).

Calcium isotopic fractionation between drip water and calcite is smaller at LSC than at WMC. $\Delta^{44}Ca$ is similar at the two Discovery Room sites with values of −0.44‰ at Discovery Room A and −0.45‰ at Discovery Room C. Both sites produce an α of 0.9996. At Fire Room $\Delta^{44}Ca$ is −0.33‰ and α is 0.9997. The mean across all LSC sites is −0.37‰ and α is 0.9996 (Table S3 in Supporting Information S1).

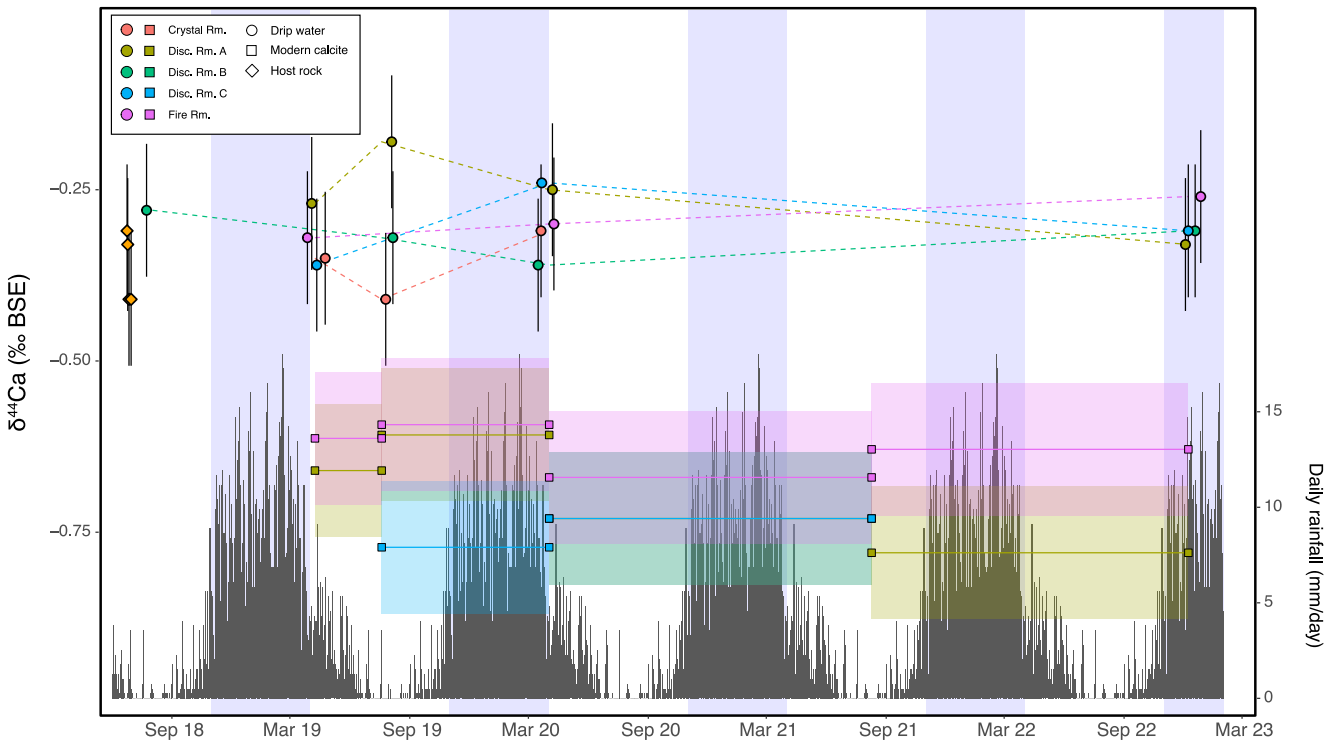

Figure 6. LSC host rock, drip water, and modern calcite $\delta^{44}Ca$ data and daily rainfall totals from the Whiskeytown UC IPM station. Error bars for host rock and drip water data and colored shading for modern calcite data show the average external 2σ over the analysis period on NIST SRM 915a (0.1‰). Vertical shading denotes the core of the wet season at LSC (November–March).

Measurements of $\delta^{13}C$ from LSC modern calcite samples installed between February 2019 and December 2022 at Discovery Room A, Discovery Room C, and Fire Room range from −8.47‰ to −0.64‰ VPDB (mean = −5.48‰, $2\sigma = 4.35$, $n = 10$) with no clear relationship to depth from the surface (Figure 5a; Table S2).

Lake Shasta Caverns modern calcite Mg/Ca values range from 2.36 to 26.24 mmol/mol (mean = 7.75 mmol/mol, $2\sigma = 18.64$, $n = 6$), Sr/Ca values from 0.02 to 0.06 mmol/mol (mean = 0.03 mmol/mol, $2\sigma = 0.03$, $n = 6$), and Ba/Ca values from 0.01 to 0.19 mmol/mol (mean = 0.06 mmol/mol, $2\sigma = 0.13$, $n = 6$) (Figures 5b–5d, Figures S2d, S2f, and S2g in Supporting Information S1; Table S2). As with modern calcite $\delta^{13}C$, there is no clear relationship between trace element ratios and the depth of the drip site from the surface at LSC. Using mean Discovery Room A drip water and mean modern calcite trace element measurements, we calculated an Mg/Ca partition coefficient (Kd_{Mg}) of 0.28, Kd_{Sr} of 0.13, and Kd_{Ba} of 0.86. At Discovery Room C, Kd_{Mg} is 0.44, Kd_{Sr} is 0.09, and Kd_{Ba} is 0.38. At Fire Room the Kd_{Mg} is 0.08, Kd_{Sr} is 0.07, and Kd_{Ba} is 0.14 (Table S3 in Supporting Information S1).

4. Discussion

We first discuss the degree to which $\delta^{44}Ca$ covaries with traditional PCP-sensitive proxies at WMC and LSC and then describe the potential influence of non-climate related factors on $\delta^{44}Ca$ in the monitoring data set. We discuss how drip water and modern calcite $\delta^{44}Ca$ can be modeled as a Rayleigh-style fractionation process to estimate relative PCP amounts and explore the sensitivity of this model to measured variability (a) in the host rock $\delta^{44}Ca$, which is assumed to set the initial $\delta^{44}Ca$ signature of infiltrating water, and (b) in the degree of isotopic fractionation between water and calcite. Finally, we compare these PCP reconstructions with measured rainfall amounts and discuss the implications of this work for semi-quantitative paleo-hydroclimate reconstructions using fossil speleothems.

4.1. Comparisons of PCP-Sensitive Proxies

The relationship between $\delta^{44}Ca$ and other potentially PCP-sensitive proxies is complex at both WMC and LSC. For both caves, we calculate correlation coefficients for modern calcite and drip waters separately using data

Table 1
Spearman's Rank Correlation Coefficient (ρ) for $\delta^{44}Ca$ Versus $\delta^{13}C$, Mg/Ca, Sr/Ca, and Ba/Ca From WMC and LSC Drip Waters and Modern Calcite

	Drip water			Modern calcite		
	Spearman's ρ	p	n	Spearman's ρ	p	n
WMC						
$\delta^{13}C$	−0.04	0.906	14	−0.35	0.18	16
Mg/Ca	−0.04	0.876	17	**0.77**	**0.003**	**13**
0.28Sr/Ca	0.28	0.281	17	**0.68**	**0.015**	**13**
Ba/Ca	−0.44	0.080	17	**0.80**	**0.002**	**13**
LSC						
$\delta^{13}C$	0.47	0.068	16	−0.16	0.649	10
Mg/Ca	−0.61	0.01	17	**−0.87**	**0.024**	**6**
Sr/Ca	0.13	0.639	17	**−0.93**	**0.050**	**6**
Ba/Ca	−0.43	0.093	17	**−0.93**	**0.008**	**6**

Note. Spearman's ρ values for which the p value is equal to or less than 0.05 are bolded.

combined from all drip sites to assess these relationships at a cave system-wide scale, though non-PCP related differences between drip sites may complicate these comparisons. There is a statistically significant positive relationship for WMC $\delta^{44}Ca$ versus Mg/Ca ($\rho = 0.77$, $p = 0.003$), Sr/Ca ($\rho = 0.68$, $p = 0.015$), and Ba/Ca ($\rho = 0.80$, $p = 0.002$) in calcite samples but not for drip water samples (Table 1; Figure 3). The lack of positive correlation between drip water trace elements and $\delta^{44}Ca$ at a cave wide level may be due in part to differences in the range of trace element data between individual drip sites. Some individual drip sites display a positive correlation between drip water trace element ratios and $\delta^{44}Ca$ (e.g., WMC4 Mg/Ca vs. $\delta^{44}Ca$), while others show a flat or negative relationship (e.g., WMC1 Mg/Ca vs. $\delta^{44}Ca$).

Positive correlations between Mg/Ca, Sr/Ca, Ba/Ca, and $\delta^{44}Ca$ measured in cave waters and carbonates are often interpreted as indicative of a dominant PCP control on these geochemical tracers (Fairchild & Treble, 2009; Owen et al., 2016). The theoretical slopes indicative of PCP for the trace element cross plots are defined by the ratio of partition coefficients of each element between calcite and water (Kd) for each element (Sinclair et al., 2012; Warken et al., 2019). Calcite Kd values depend on multiple factors, including temperature, growth rate, and the trace element ratio of water and the calcite that is being formed (Wassenburg et al., 2020). Laboratory studies have reported a negative relationship between Kd_{Mg} and fluid Mg/Ca and calcite growth rate and a positive relationship with temperature (Day & Henderson, 2013; Huang & Fairchild, 2001; Mucci & Morse, 1983). Calcite Kd_{Sr} has been shown to increase with increasing growth rates and the calcite Mg/Ca ratio (Gabitov et al., 2014; Mucci & Morse, 1983; Tesoriero & Pankow, 1996). Similarly, Kd_{Ba} has been shown to increase with increasing growth rates (Tesoriero & Pankow, 1996).

Using the paired calcite and drip water data available, we calculate partition coefficients for each element (Mg, Sr, Ba) at both cave sites (Table S2). WMC1 and WMC3 Kd_{Mg} and Kd_{Sr} values are within the range provided by Sinclair et al. (2012) for a compilation of tropical speleothems (0.013–0.06 for Kd_{Mg} 0.057–0.3 for Kd_{Sr}) and comparable to the range provided by Wassenburg et al. (2020) for speleothems from a range of climatological and geologic settings (0.011–0.039 for Kd_{Mg} and 0.037–0.34 for Kd_{Sr}). WMC4 and WMC6 Kd_{Mg} and Kd_{Sr} values are higher than those for WMC1 and WMC3 and outside the ranges observed in Sinclair et al. (2012) and Wassenburg et al. (2020). Kd_{Ba} values for all WMC drip sites are higher than has been observed in laboratory studies (0.003–0.053) (Tesoriero & Pankow, 1996). WMC4 and WMC6 display Kd_{Ba} values of above 1, reflecting a higher Ba/Ca in modern calcite than in the drip water samples.

Wassenburg et al. (2020) observed a strong positive relationship between Kd_{Sr} and calcite Mg/Ca in speleothem samples, so the higher calcite Mg/Ca in WMC4 and WMC6 samples may contribute to the higher Kd_{Sr} at these sites. However, it is difficult to reconcile Kd_{Mg} and Kd_{Ba} values that far exceed ranges previously reported for laboratory studies and speleothem samples based on environmental or elemental variability alone. Instead, since the glass plates were not seeded with calcite prior to deployment, the calculation of these Kd values may be related to the mixing of initial, non-seeded calcite growth, which can display an atypical chemical signature and obfuscate a clear picture of elemental partitioning (Day & Henderson, 2013; Tesoriero & Pankow, 1996). The influence of non-seeded calcite may be especially relevant for Kd_{Ba} since Ba concentrations are lower overall than Mg or Sr. Furthermore, the amount of calcite recovered from WMC4 and WCM6 plates tended to be lower than for WMC1 and WMC3, potentially increasing the relative influence of non-seeded calcite on modern calcite Ba/Ca at these deeper sites with the highest and most anomalous Kd_{Ba}.

Additionally, uncertainties in the calculation of Kd values and deviations from theoretical PCP slopes in the modern calcite data may be related to solution mixing between incoming drip water and the thin film of water on the glass plate and/or mixing of solids formed from solutions that have experienced different growth rates and/or amounts of PCP, which can complicate a clear PCP signal. This has been observed in laboratory studies (Day & Henderson, 2013). These mixing effects are likely maximized when a plate contains calcite grown during both wet and dry intervals, as is the case for these highly seasonal CA caves systems. Solid-mixing and non-seeded

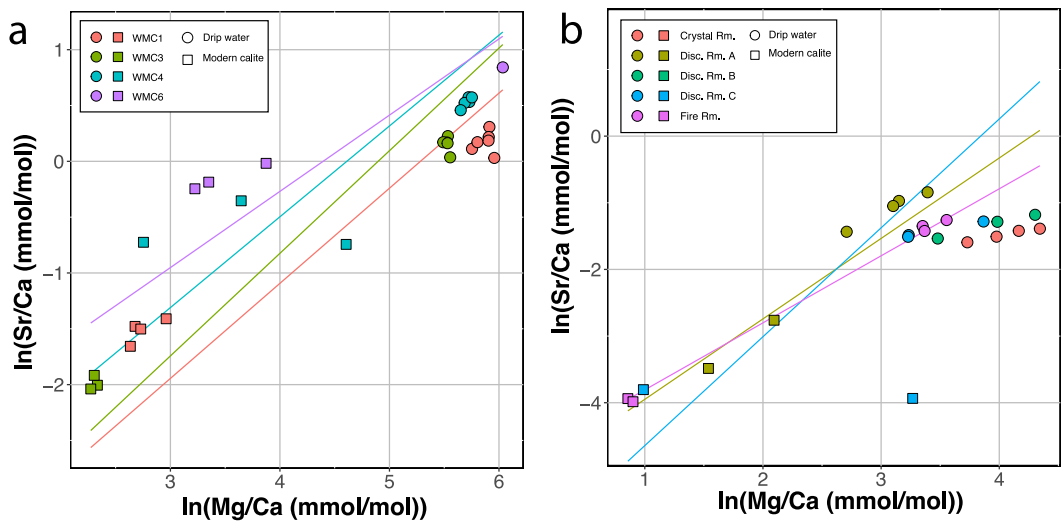

Figure 7. Cross plots of WMC drip water and modern calcite ln(Mg/Ca mmol/mol) versus ln(Sr/Ca mmol/mol) (a), WMC ln (Sr/Ca mmol/mol) versus ln(Ba/Ca mmol/mol) (b), LSC drip water and modern calcite ln(Mg/Ca mmol/mol) versus ln(Sr/Ca mmol/mol) (c), and LSC ln(Sr/Ca mmol/mol) versus ln(Ba/Ca mmol/mol) (d). Solid lines show theoretical prior calcite precipitation slopes based on Kd values calculated for each site.

growth should not influence stalagmite or drip water data and thus may be particularly relevant to the modern calcite data.

Since WMC Kd_{Mg} and Kd_{Sr} are within or comparable to previously published data, we used these data to calculate theoretical PCP slopes for individual WMC drip sites. We calculated ln(Sr/Ca) versus ln(Mg/Ca) slopes of 0.85, 0.92, 0.81, and 0.68 at WMC sites WMC1, WMC3, WMC4, and WMC6, respectively (Figure 7a). These ln(Sr/Ca) versus ln(Mg/Ca) slopes are within the range provided by Sinclair et al. (2012) based on a compilation of tropical speleothems (0.707–1.003) and WMC drip water and modern calcite samples tend to plot near to the site-specific theoretical PCP relationships, though there are some deviations, such as WMC4 modern calcite (Figure 7a). Site WMC4 also displays an almost ten-fold change in modern calcite Mg/Ca across the three samples, a larger range than any of the other WMC sites. This large range in Mg/Ca further suggests that Mg/Ca variability at this site is not driven solely by PCP but rather by a combination of PCP and variability in the contribution of Mg from the host rock.

We also compared Sr and Mg concentrations ([Sr] and [Mg]) to assess source variability between Sr and Mg at different drip sites (Tremaine & Froelich, 2013). At WMC, drip water [Sr] versus [Mg] shows distinct clusters that correspond to each drip site and the shallower WMC1 and WMC3 sites plot along a similar linear slope that is steeper than that of the deeper WMC4 and WMC6 sites (Figure S3a in Supporting Information S1). Similarly, WMC1 and WMC3 modern calcite [Sr] versus [Mg] cluster more tightly and plot along a steeper slope than WMC4 and WMC6 modern calcite [Sr] versus [Mg] (Figure S3b in Supporting Information S1). This indicates that Sr and Mg are likely supplied by a consistent source at WMC1 and WMC3 and that PCP is a driver of Sr/Ca and Mg/Ca variability (Tremaine & Froelich, 2013). The deeper WMC4 and WMC6 sites are likely characterized by a different, and perhaps more variable, Sr and Mg source, with trace element ratios at these sites potentially reflecting a combination of PCP and variability in the contribution of Mg-rich phases in the host rock.

These comparisons indicate that there is likely to be a shared influence of PCP for $\delta^{44}Ca$ and trace element ratios at WMC at the time scale represented by the calcite samples, though the deviations from the theoretical PCP slopes and [Sr] versus [Mg] slopes, such as at site WMC4, indicate that PCP may not be the only control on trace element ratios at sites deeper in the cave (Figure 7a; Figures S3a and S3b in Supporting Information S1). This is consistent with a record of Mg/Ca from a WMC stalagmite found at a level similar to sites WMC4 and WMC6, which is interpreted to represent a combination of both PCP and changes in the dissolution of Mg-rich phases in host rock (de Wet et al., 2021; Oster et al., 2017). However, the lack of a positive correlation between WMC drip water and modern calcite $\delta^{44}Ca$ and $\delta^{13}C$ (Figure 3a) is not consistent with WMC stalagmite data, which shows a positive correlation between $\delta^{44}Ca$ and $\delta^{13}C$, indicative of a shared PCP control (de Wet et al., 2021). This may

arise because the monitoring samples record seasonal variability in $\delta^{13}C$ driven by soil processes, while the decadal-scale variations in the stalagmite $\delta^{13}C$ are more influenced by PCP. It may also be the case that the various WMC drip sites record $\delta^{13}C$ differently than the site from which the stalagmite was collected or that the modern calcite data is impacted by solution- or solid-mixing during calcite growth and sampling.

With the exception of LSC drip water $\delta^{13}C$, which shows a moderate but not significant positive relationship ($\rho = 0.47$, $p = 0.068$), the relationships between LSC modern calcite and drip water $\delta^{44}Ca$ and $\delta^{13}C$ and trace elements generally do not show a positive correlation that would be indicative of a shared PCP control when modern calcite and drip water data are combined from each site (Table 1; Figure 5). Instead, there appears to be a negative relationship between Mg/Ca, Sr/Ca, Ba/Ca, and $\delta^{44}Ca$ in calcite. However, some sites do qualitatively display positive relationships between drip water trace element ratios and $\delta^{44}Ca$, such as Discovery Room A, indicating variability in the role of PCP in determining drip water chemistry between different LSC drip sites.

Similar to WMC, we observe variability in trace element Kd values between different LSC drip sites (Table S2). LSC site-specific Kd_{Sr} values are within the range reported in previous laboratory and speleothem studies, while Kd_{Mg} values are slightly higher than has been previously reported (Table S2) (Sinclair et al., 2012; Wassenburg et al., 2020). LSC Kd_{Ba} values are also higher than the range reported in Tesoriero and Pankow (1996), but not to the same extent as those from WMC4 and WMC6. As with WMC, it is possible that mixing of initial, non-seeded calcite growth characterized by a different Kd with later calcite may play a role in the LSC Kd values, especially Kd_{Ba}, which is an order of magnitude higher than values in Tesoriero and Pankow (1996) for calcite that was corrected for the content of seeded material. For this reason, we use ln(Sr/Ca) versus ln(Mg/Ca) to calculate theoretical PCP slopes for individual LSC drip sites that have paired modern calcite and drip water data (Figure 7b). LSC ln(Sr/Ca) versus ln(Mg/Ca) slopes are 1.21, 1.6, and 1 for Discovery Room A, Discovery C, and Fire, respectively. These slopes are above the range reported for tropical speleothems in Sinclair et al. (2012) (1.003), but all but 1.6 are below the upper limit modeled for speleothems from a wider range of climatic and geological settings (1.45) in Wassenburg et al. (2020). Trace element ratios from Discovery Room A show relatively good coherence with the theoretical PCP relationship. The Fire Room may as well, though the range of variability in Mg/Ca and Sr/Ca is low at this site. Discovery Room C modern calcite samples show a large spread around the PCP slope, suggesting that PCP is not a main driver of trace element variability at this site (Figure 7b).

Unlike WMC, LSC drip water [Sr] versus [Mg] data from different sites do not plot along similar slopes. There is a non-linear spread at all sites except for Discovery Room A and Discovery Room B, which graphically show linear relationships between [Sr] and [Mg] that would be characteristic of a single Sr and Mg source and a strong PCP signal but with different slopes (Tremaine & Froelich, 2013) (Figure S3b in Supporting Information S1). More LSC modern calcite data would be needed to fully assess [Sr] and [Mg] in calcite at these drip sites. The lack of clear linear relationships in LSC drip water [Sr] versus [Mg] points to variable Sr and Mg sources between sites and within individual sites through time (Figure S3b in Supporting Information S1).

A non-dominant role for PCP in LSC trace element data is consistent with trace element data from LSC stalagmite records, which have been interpreted as reflecting a combination of PCP and contributions to seepage water from soil inputs and variable host rock dissolution (Oster et al., 2020). Oster et al. (2020) identified changes in water supply and the resulting influence on soil processes and degassing in the epikarst as the primary controls on stalagmite $\delta^{13}C$, which should result in tight coupling of the $\delta^{44}Ca$ and $\delta^{13}C$ data. This may be consistent with the relationship between LSC drip water $\delta^{13}C$ and $\delta^{44}Ca$ but is not borne out in the modern calcite data (Figure 5a). As with WMC, this may be related to the shorter timescales represented in the monitoring data relative to the stalagmite record, variability in the processes that control $\delta^{13}C$ records between different drip sites, or the influence of solution- or solid-mixing on the modern calcite data.

These comparisons indicate that while PCP is likely to be an important control on drip water and modern calcite, and thus speleothem, geochemistry, other environmental and sampling factors contribute to trace element and $\delta^{13}C$ variability to various degrees across both cave systems. At LSC, speleothem $\delta^{44}Ca$ may be a more reliable proxy for PCP at the timescale of the monitoring data, with drip water and modern calcite demonstrating multiple environmental controls on trace element ratios and $\delta^{13}C$. These findings confirm that future paleoclimate reconstructions using speleothems should strongly consider the degree to which trace element ratios represent PCP alone, as opposed to a combination of PCP and other infiltration-related parameters, such as soil contributions or incongruent host rock dissolution (Fairchild & Treble, 2009). However, it should also be noted that factors besides PCP (e.g., variability in host rock $\delta^{44}Ca$ or in the Ca isotopic fractionation factor) may also impact $\delta^{44}Ca$.

4.2. Non-Climate Factors Affecting Ca Isotopes in Cave Systems

To investigate how non-climate factors may influence cave system $\delta^{44}Ca$ values we compare coeval $\delta^{44}Ca$ measurements from different drip sites within each cave. Assuming that depth within the cave system correlates to water flow path length, the comparison of shallower versus deeper sites allows for the influence of flow path length through the vadose zone on PCP potential to be assessed independently of rainfall rates. However, it is important to note that the water flow path type (e.g., matrix vs. fracture flow) and abundance of pore space along the flow path will impact the relative PCP potential between different drip sites in addition to flow path length (e.g., Oster et al., 2021). Thus, depth from the surface should only be a significant modulator of PCP only when these other characteristics are consistent.

At WMC, all drip sites display qualitatively similar flow characteristics (e.g., similar response time to rain events, large seasonal variability in drip rate), but sites WMC4 and WMC6 are ∼50 m further from the surface than sites WMC1 and WMC3. Modern calcite grown at these two deeper sites displays generally less negative $\delta^{44}Ca$ values (T Test p value = 0.08) and generally higher modern calcite Mg/Ca values relative to the shallower sites (T Test p value = 0.063). This may indicate greater amounts of PCP occurring at the deeper sites, though these depth relationships are less clear in the drip water data.

At LSC, the Discovery Room and Fire Room drip sites also displayed qualitatively similar drip characteristics. The difference in depth from the surface between these two drip sites is only ∼10 m, but the deeper site (Fire Room, ∼40 m from surface) does show less negative modern calcite $\delta^{44}Ca$ values relative to the Discovery Room sites (T Test p value: 0.027). These data indicate that the deeper cave sites may experience a longer flow path through the vadose zone (Figures 2b and 2c), allowing more opportunity for CO_2 degassing and PCP than the shallower sites under the same climate conditions. This supports the conceptual model of PCP controls on cave system $\delta^{44}Ca$ (Figure 1) and indicates that PCP reconstructions from stalagmites should be calibrated with measurements from drip sites from the same or comparable depths.

The Crystal Room drip site is distinct in LSC because it drips throughout the year, even in the summer when most other LSC sites are at least intermittently dry (Dave Mundt, personal communication). This indicates that the Crystal Room is fed by a consistent and year-round reservoir of water in the karst. Drip water $\delta^{44}Ca$ from Crystal Room tends to be more negative than other LSC drip sites and the most negative value (−0.41‰ on 6/7/19) is equal to the two most negative LSC host rock $\delta^{44}Ca$ measurements (Figure 4, Figure S2a in Supporting Information S1). This indicates that the host rock contribution is likely best represented by the most negative end-member and/or is not fully constrained for this drip site, and that Crystal Room drip waters experience little to no PCP regardless of season. In this case, Crystal Room drip $\delta^{44}Ca$ values are likely not suitable for reliable reconstructions of PCP.

4.3. Quantitative PCP Reconstructions Using Ca Isotopes

Since the lighter ^{40}Ca isotope preferentially enters the solid phase during carbonate formation, drip waters that have undergone PCP during infiltration from the surface should display less negative $\delta^{44}Ca$ values relative to the cave host rock, which is assumed to be the source of the initial water $\delta^{44}Ca$ signature (Figure 1; de Wet et al., 2021; Owen et al., 2016; Reynard et al., 2011). We observed drip water $\delta^{44}Ca$ values that were more enriched in the heavier ^{44}Ca isotope relative to the median host rock value across all WMC samples and the majority of LSC samples. This suggests that a PCP signal in cave system $\delta^{44}Ca$ is resolvable on an annual to sub-annual scale in these cave systems.

The degree of PCP-driven drip water enrichment in ^{44}Ca at WMC and LSC is less than has been reported for drip waters from Heshang Cave, China (Figure 8). PCP-driven enrichment in ^{44}Ca in WMC drip waters is comparable to that of measured drip waters from Mawmluh Cave, India. LSC displays drip water values that are closer to respective host rock values, which may indicate less PCP-driven isotopic enrichment in this system (Figure 8). For comparison, we also show $\delta^{44}Ca$ data from an aragonite stalagmite from Dharamjali Cave, India, as well as from one drip water, two modern calcite, and one host rock sample (Giesche et al., 2023) and $\delta^{44}Ca$ data from three stalagmites and three isotopically identical host rock samples from El Pindal and La Vallina Caves that formed within the same limestone unit in the northwestern Iberian Peninsula (Lechleitner et al., 2021; Stoll et al., 2023), both of which show PCP-driven enrichment in carbonate ^{44}Ca relative to the host rock (Figure 8).

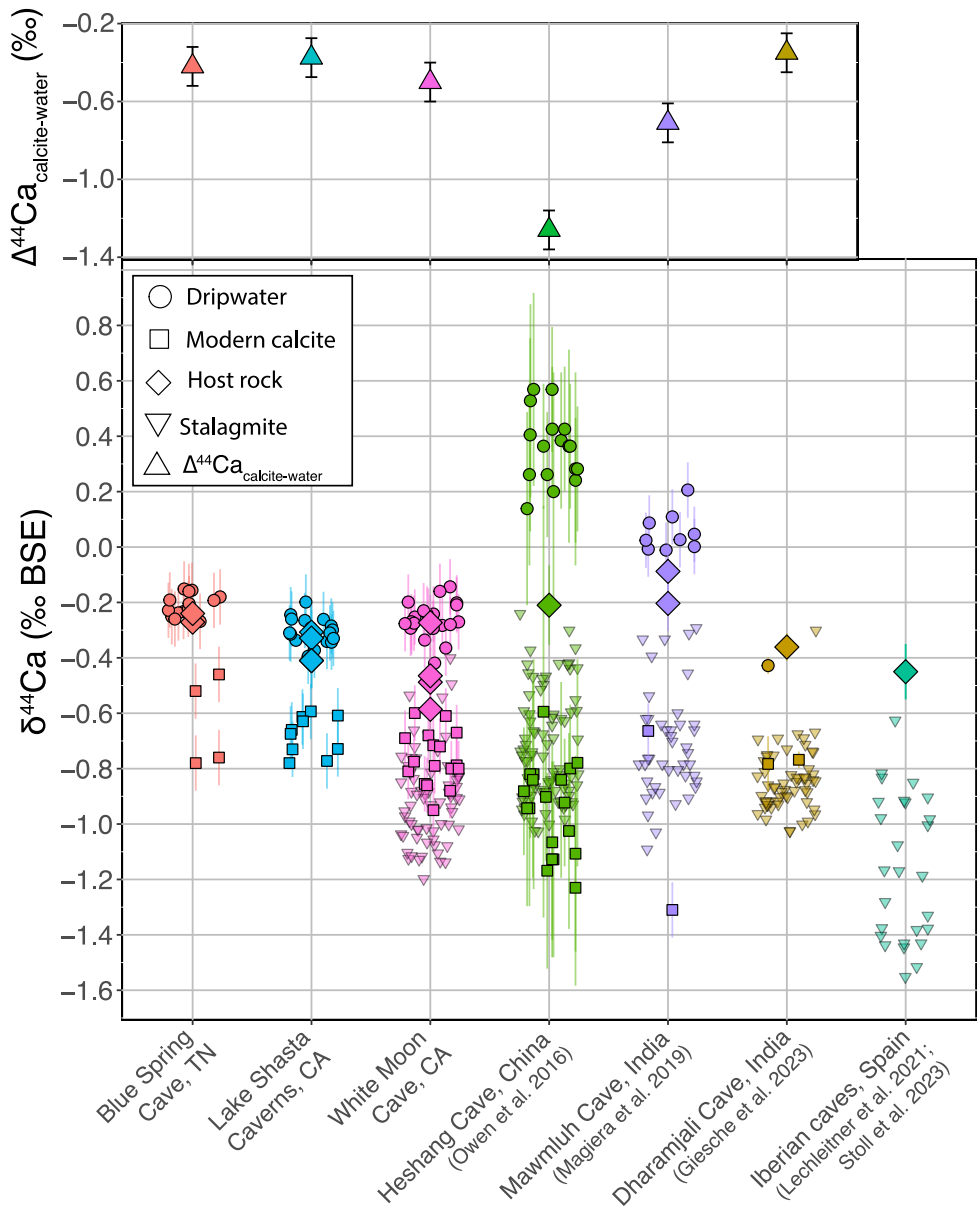

Figure 8. Distribution of drip water, cave carbonate, and carbonate host rock $\delta^{44}Ca$ data from Blue Spring Cave (unpublished data from de Wet (2023)), Lake Shasta Caverns (LSC) and White Moon Cave (WMC) (this study, de Wet et al., 2021), Heshang Cave (Owen et al., 2016), Mawmluh Cave (MAW) (Magiera et al., 2019), Dharamjali Cave (DHAR) (Giesche et al., 2023), and Iberian caves (El Pindal and La Vallina Caves) (Lechleitner et al., 2021; Stoll et al., 2023). Ca isotope fractionation values between calcite and water ($\Delta^{44}Ca$) are shown for the caves for which drip water and modern calcite $\delta^{44}Ca$ measurements have been reported. BSC, LSC, DHAR, MAW, and the Iberian Caves developed in limestone host rock, WMC developed in marble host rock, and Heshang Cave developed in dolomite host rock.

The fraction of the amount of Ca dissolved from the host rock that remains in solution when infiltrating water reaches the drip site or stalagmite (f) can be quantified using transfer functions that describe the evolution of Ca isotopes during PCP as a Rayleigh fractionation process (Owen et al., 2016). Cave drip water and speleothem carbonate allow for the calculation of Ca isotope fractionation between the fluid and solid phase $\Delta^{44}Ca_{calcite\text{-}wate}$:

$$\Delta^{44}Ca_{calcite-water} = \delta^{44}Ca_{calcite} - \delta^{44}Ca_{water} \quad (2)$$

which can be expressed as an effective fractionation factor (α):

$$\alpha_{\text{calcite-water}} = \frac{1000 + \delta_{\text{calcite}}}{1000 + \delta_{\text{water}}} \quad (3)$$

and used to calculate f for drip water (Equation 4) or calcite (Equation 5):

$$f_{\text{water}} = \left(\frac{r_d}{r_0}\right)^{\frac{1}{\alpha-1}} \quad (4)$$

$$f_{\text{calcite}} = \left(\frac{r_s}{\alpha * r_0}\right)^{\frac{1}{\alpha-1}} \quad (5)$$

Here, r_d is the Ca isotope ratio in the drip water when it reaches the drip site ($r_d = \delta_{\text{water}}/1{,}000 + 1$), r_s is the Ca isotope ratio in the speleothem or modern calcite ($r_s = \delta_{\text{calcite}}/1{,}000 + 1$), and r_0 is the initial Ca isotope ratio in the dripwater ($r_0 = \delta_{\text{dripwater}}{}^{f\,=\,1}/1{,}000 + 1$), which is assumed to be the same as the measured host rock value.

4.3.1. Host Rock δ^{44}Ca Variability

Previous studies have measured the δ^{44}Ca signature of one or two hand samples of cave host rock (Giesche et al., 2023; Lechleitner et al., 2021; Magiera et al., 2019; Owen et al., 2016) and assumed that the contribution of host rock δ^{44}Ca is invariable through time. However, de Wet et al. (2021) report variability in δ^{44}Ca of ~0.32‰ across three host rock samples from WMC, with implications for f values that are reconstructed from stalagmite δ^{44}Ca. To explore the sensitivity of drip water and modern calcite PCP reconstructions to variability in host rock δ^{44}Ca we use Equations 4 and 5 with measured values of δ^{44}Ca for four host rock samples from both LSC and WMC (Figure 9).

The range of measured WMC host rock δ^{44}Ca values produces f values that vary by almost 0.5, which would correlate to a difference in reconstructed PCP of up to 50%, with higher f values corresponding to the least negative host rock δ^{44}Ca value (Figure 9a). Using the cave-wide α (0.9995) and the median host rock δ^{44}Ca value (−0.48‰) for WMC, we calculated a mean drip water f value of 0.65 (i.e., 35% Ca removal via PCP) (Equation 4) and a mean modern calcite f value of 0.66 (Equation 5, Figure 9a). Using the cave-wide α and the minimum WMC host rock δ^{44}Ca value (−0.59‰), we calculated mean f values for WMC drip water and modern calcite of 0.52 and 0.53 respectively. Using the cave-wide α and the maximum WMC host rock δ^{44}Ca value (−0.27‰), we calculated mean f values for WMC drip water and modern calcite of 0.99 and 1.00 respectively.

The range of δ^{44}Ca variability in measured LSC host rock samples is less than that of WMC and is within the average external 2σ on NIST 915B over the analysis period. Nonetheless, the range of measured LSC host rock values results in a shift in the mean calculated f values of ±0.1, or roughly 10% more or less average PCP, relative to calculations using the median host rock value. Using the cave-wide α (0.9996) and the median host rock δ^{44}Ca value (−0.37‰) for LSC, we calculated a mean drip water f value of 0.83 (i.e., 17%) Ca removal via PCP (Equation 4) and a mean modern calcite f value of 0.81 (Equation 5; Figure 9c). The cave-wide α and the minimum LSC host rock value δ^{44}Ca (−0.41‰) yield mean values of 0.75 and 0.73 for LSC drip water and modern calcite, respectively. Conversely, the cave-wide α and the maximum LSC host rock value δ^{44}Ca (−0.31‰) yield a mean of 0.96 and 0.94 for LSC drip water and modern calcite, respectively (Figure 9c).

This analysis shows that the range of natural variability in carbonate host rock in these cave systems can contribute considerable uncertainty to PCP reconstructions using Ca isotopes. This effect is more pronounced at WMC where the range of host rock δ^{44}Ca is greater, perhaps because the WMC host rock is a metamorphosed marble with considerable mineralogical heterogeneity at the hand sample scale. At both sites the use of the highest host rock δ^{44}Ca value yields some f values that are greater than 1, which would indicate no Ca removed via PCP and is not consistent with the Rayleigh fractionation model framework. Based on Equation 4 and Equation 5, the sensitivity to host rock δ^{44}Ca is greater for f values closer to 1, that is, for intervals when there is less PCP occurring in the system and thus more effective rainfall (Figures 9a and 9c). Considering this, the range of δ^{44}Ca variability in different types of carbonate host rocks deserves further study and should be well-constrained at a given cave site prior to generating quantitative PCP reconstructions using this Rayleigh modeling framework.

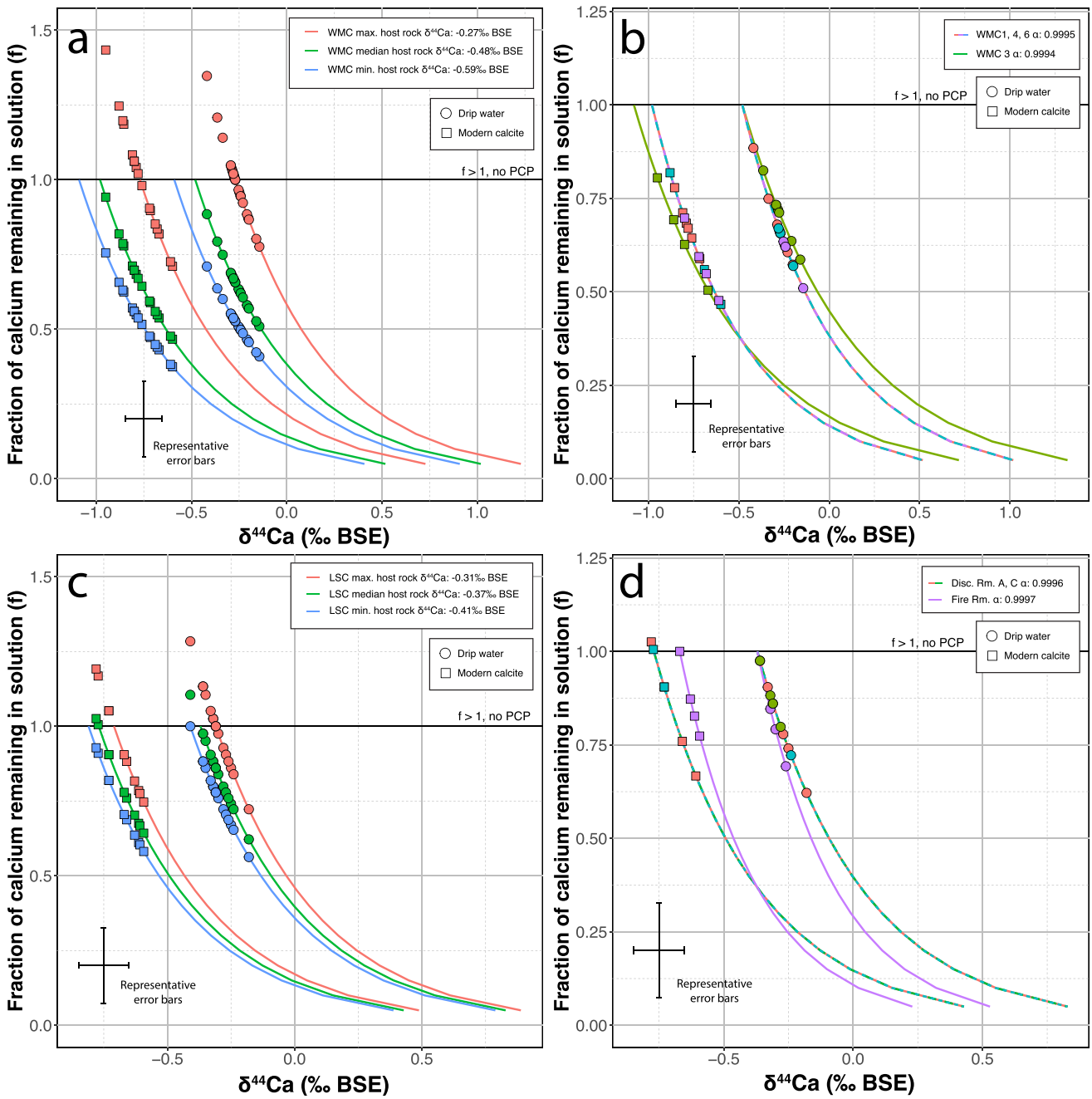

Figure 9. WMC drip water and modern calcite $\delta^{44}Ca$ versus the fraction of Ca remaining solution (f) calculated using Equations 4 and 5 using the cave-wide α (0.9995) and the maximum, minimum, and median host rock $\delta^{44}Ca$ values (a). The same as (a) except using drip site-specific α values and the median host rock the $\delta^{44}Ca$ for WMC (b). LSC drip water and modern calcite $\delta^{44}Ca$ versus the fraction of Ca remaining solution (f) calculated with Equations 4 and 5 using the cave-wide α (0.9996) and the maximum, minimum, and median host rock $\delta^{44}Ca$ values (c). The same as (c) except using drip site-specific α values and the median host rock the $\delta^{44}Ca$ for LSC (d).

4.3.2. Variability in Ca Isotopic Fractionation

In addition to testing the sensitivity of PCP reconstructions to host rock $\delta^{44}Ca$ variability, we assessed the impact of variability in the α that is used (Figures 9b and 9d). Modern calcite $\delta^{44}Ca$ values are offset from the drip water values by the degree of fractionation ($\Delta^{44}Ca$), which can be represented as an effective fractionation factor α (Equation 3). Growth rate is the dominant control on $\Delta^{44}Ca$ and is a function of calcite saturation state, and thus may vary along the flow path of infiltrating water based on conditions in the vadose zone (Owen et al., 2016; Tang

et al., 2008). However, the growth rate during PCP both in the vadose zone and at the drip site in the cave is difficult to constrain even with extensive monitoring data. Stoll et al. (2023) calculated different f values for stalagmite $\delta^{44}Ca$ using a range of $\Delta^{44}Ca$ based on laboratory studies; but, aside from de Wet et al. (2021), previous work has not looked closely at the sensitivity of PCP reconstructions using different $\Delta^{44}Ca$ measured from cave monitoring data from multiple drip sites. Considering this and using an updated WMC data set and new LSC monitoring data, we calculate $\Delta^{44}Ca$ and α for each individual drip site that has paired drip water and calcite measurements as well as for both cave systems as a whole using a combination of measurements from all the drip sites. Drip water data may represent an aggregated signal depending on water mixing and residence time in the vadose zone but is sampled at one particular moment in time. Modern calcite from glass plates integrates an average signal from the entire interval over which the calcite precipitates. We used the means of these measurements to broadly characterize Ca isotopic fractionation in the monitoring data sets.

At WMC, sites WCM1, WMC4, and WMC6 produce $\Delta^{44}Ca$ values of −0.5‰, −0.47‰, and −0.44‰ respectively, and α values that are indistinguishable from the mean of all the data from all the drip sites (0.9995). Site WMC3, however, is characterized by the most negative $\Delta^{44}Ca$ value (−0.55‰) and a lower α (0.9994) than that of the mean of all sites. The more negative $\Delta^{44}Ca$ at WMC3 and, to a lesser extent, WMC1 is consistent with these sites displaying lower [Ca] values (Table S2) and lower pCO_2 (Table S1 in Supporting Information S1) due to their proximity to the cave entrance, providing more potential for CO_2 degassing and faster growth rates (Stoll et al., 2012; Tang et al., 2008). Using the median WMC host rock $\delta^{44}Ca$ value (−0.48‰) and the site-specific α (0.9994) for WMC3, we calculated a mean drip water f value (0.71) that is 0.05 higher than that for the cave-wide α (0.66) and a mean modern calcite f value (0.66) that is 0.08 lower than that for the cave-wide α (0.74) (Figure 9b). This shows the sensitivity of the calculations of f to measured differences in isotope fractionation between WMC drip sites.

At LSC, both Discovery Room A and Discovery Room C, which are ∼10 m apart in the same room of the cave, produce $\Delta^{44}Ca$ values of −0.44 and −0.45 respectively and α of 0.9996, which are indistinguishable from the α calculated with the mean of all LSC drip water and calcite samples. However, the Fire Room, which is ∼10 m deeper than the Discovery Room, displays a less negative $\Delta^{44}Ca$ (−0.33) and α of 0.9997, higher than that of the Discovery Room sites (0.9996). This suggests a slower calcite growth rate at the Fire Room site, consistent with generally higher pCO_2 levels at this deeper site (Tang et al., 2008). Using the median LSC host rock $\delta^{44}Ca$ value (−0.37‰) and this site-specific α for Fire Room (0.9997), we calculated a mean drip water f value of 0.78 (i.e., 22% Ca removal via PCP) (Equation 4) and a mean modern calcite f value of 0.88 (i.e., 12% Ca removal via PCP) (Equation 5). This drip water f value is 0.05 lower than the mean calculated for the Fire Room site with the cave-wide α (0.83), while the modern calcite f value is 0.18 higher than the mean calculated for the Fire Room site with the cave-wide α (0.70) (Figure 9d).

For comparison with drip site-specific $\Delta^{44}Ca$ and α values, we calculated trace element partition coefficients (Kd_{Mg}, Kd_{Sr}, and Kd_{Ba}) for each drip site that has paired modern calcite data (Figure S4; Table S3 in Supporting Information S1). Laboratory experiments show a positive relationship between absolute $\Delta^{44}Ca$ values and Kd_{Sr} in inorganic calcite and suggest that both Sr and ^{44}Ca incorporation are similarly controlled by the mechanism of growth entrapment (Tang et al., 2008). At WMC, lower Kd_{Mg} and Kd_{Sr} values correspond to more negative $\Delta^{44}Ca$ values, with WMC4 and WMC6 displaying the highest Kd_{Mg} and Kd_{Sr}. This is the opposite of the positive relationship between absolute $\Delta^{44}Ca$ values and Kd_{Sr} found by Tang et al. (2008), perhaps suggesting that the growth mechanics that characterize these cave samples differ from those of laboratory settings. Conversely, Kd_{Mg} at WMC4 and WMC6 is lower than at the shallower sites WMC1 and WMC3. At LSC the site with the least negative $\Delta^{44}Ca$ (Fire Room) yields the lowest Kd_{Mg} and Kd_{Sr}, consistent with the relationship from Tang et al. (2008) for Kd_{Sr}, though the difference in Kd_{Sr} between the LSC sites is small (Figure S4 in Supporting Information S1).

It is not unexpected that trace element Kd values and $\Delta^{44}Ca$ varies between drip sites and over time at individual sites if the flow rate through the vadose zone, calcite saturation state of the drip water, and/or calcite growth rate are not consistent in time or space. We demonstrate measurable variability in $\Delta^{44}Ca$ between drip sites in our multi-year monitoring data set and show that a change in the α that is applied to a drip site of only 0.0001 results in shifts in the amount PCP recorded by cave carbonate of up to ∼0.15 (i.e., 15% more or less Ca removal via PCP) at WMC and ∼0.19 (i.e., 19% more or less Ca removal) at LSC for the samples with largest f values. This sensitivity is greater for higher f values in the case of carbonate (Equation 5) and greater for lower f values in the case of drip

water (Equation 4) (Figures 9b and 9d). Importantly, this sensitivity for carbonate is also greater for smaller Δ^{44}Ca, which is likely to be the case for caves with slow calcite precipitation rates such as these California caves. We measure Δ^{44}Ca values for WMC and LSC that are less negative than those reported or modeled in previous studies (Owen et al., 2016; Stoll et al., 2023), likely due to slower calcite growth rates at WMC and LSC, so the Rayleigh fractionation slopes that characterize these systems are steeper than those modeled for the La Vallina or Heshang Cave systems.

It can be difficult to fully constrain Δ^{44}Ca in modern systems because of the different temporal resolution of modern calcite and drip water samples. Here, we use a multi-year spatially comprehensive monitoring data set to constrain Δ^{44}Ca and find that it may be useful to aggregate data from multiple drip sites to increase the number of observations. However, this should perhaps only be done if the sites are reasonably similar in terms of calcite growth characteristics, as appears to be the case, for example, for the Discovery Sites at LSC but not for the Fire Room.

4.3.3. Calculated *f* Values That Are Greater Than 1

At LSC, PCP reconstructions using the median and least negative host rock δ^{44}Ca values produce *f* values close to or greater than 1, as do PCP reconstructions at WMC using the least negative host rock δ^{44}Ca value (Figure 9). The calculation of *f* values at or greater than 1 indicates little to no PCP occurring when that sample was taken. This has been reported for stalagmite δ^{44}Ca records from Mawmluh Cave, India (Magiera et al., 2019), WMC (de Wet et al., 2021), and La Vallina Cave depending on the assumed Δ^{44}Ca (Stoll et al., 2023). It is not unexpected to see *f* values close to or equal to 1 in monitoring data, especially in systems like WMC and LSC that are prone to fast-paced infiltration in the form of fracture flow in response to rainfall events. However, the calculation of *f* values much greater than 1 is not consistent with the Rayleigh fractionation modeling framework, which assumes the carbonate host rock δ^{44}Ca value to be representative of the drip water δ^{44}Ca value when no PCP has occurred (i.e., when $f = 1$). If a stalagmite δ^{44}Ca record produces many *f* values that are greater than 1 by a larger magnitude than analytical uncertainty, then the cave system may not be adequately constrained in terms of the contribution of δ^{44}Ca from the host rock or other potential sources to the stalagmite (i.e., initial δ^{44}Ca) or the fractionation factor, both of which have a greater effect on stalagmite *f* when *f* is close to 1. In the case of LSC, the application of the Fire Room α value to modern calcite data from Discovery Room increases the *f* values that are calculated and produces *f* values greater than 1 for three of the five samples, while the use of site-specific α values produces *f* values that are all less than 1 (Figure 9d).

4.4. Reconstructed PCP Versus Rainfall and Implications for Quantitative Paleoclimate Reconstructions From Speleothems

To explore quantitative rainfall reconstructions from δ^{44}Ca PCP estimates, we compare mean PCP reconstructed from drip water and modern calcite samples with the mean rainfall rates over the monitoring period at each cave. WMC experienced an average of 0.9 mm/day of rainfall from March 2017 to December 2022, and the average PCP estimated from drip water and calcite δ^{44}Ca is 35%. LSC experienced an average of 4.3 mm/day of rainfall between February 2019 and December 2022 and the average PCP estimated over this interval is 16% (Figure 10). In addition to being drier, WMC is a deeper cave than LSC, which may provide more opportunity for PCP. However, the Fire Room, the deepest site at LSC, is characterized by consistently less PCP than the shallowest sites at WMC. This indicates that the difference in reconstructed PCP between LSC and WMC is unlikely to be solely the result of the different cave depths but is instead likely related to the drier hydroclimate conditions at WMC over the monitoring period.

We also compare the reconstructed PCP rates from WMC and LSC modern calcite samples with the amount of rainfall that occurred during the interval over which the calcite formed to investigate this relationship at a roughly annual scale (Figure 11). The modern calcite samples can be considered analogous to short intervals of fossil speleothem growth and should represent a mean PCP signal for the calcite growth period, though this may be complicated by variability in the calcite growth rate and non-linearities in PCP response to rainfall events (de Wet et al., 2021; Owen et al., 2016). We use rainfall sums instead of daily averages because rainfall is highly seasonal at both sites and drip rates tend to slow to zero during the dry summer months (de Wet et al., 2021). Daily rainfall rates incorporate periods when no rainfall occurs, and drip rates and calcite precipitation cease and may thus skew the comparison.

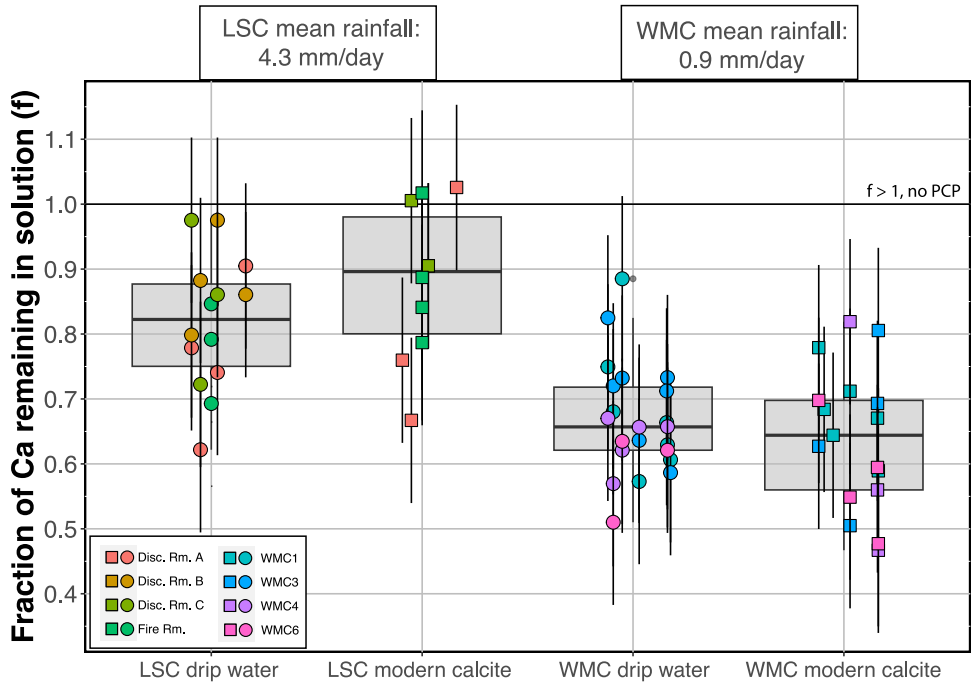

Figure 10. LSC and WMC drip water and modern calcite *f* values were calculated using drip site-specific α and the median host rock $\delta^{44}Ca$ values.

There is a positive correlation between modern calcite *f* values and rainfall amounts across the WMC and LSC data ($\rho = 0.73$, *p*-value = <0.01), indicating a strong rainfall control on PCP in these systems (Figure 11). At WMC, site WMC1 has been monitored the longest and shows a generally positive relationship between *f* values

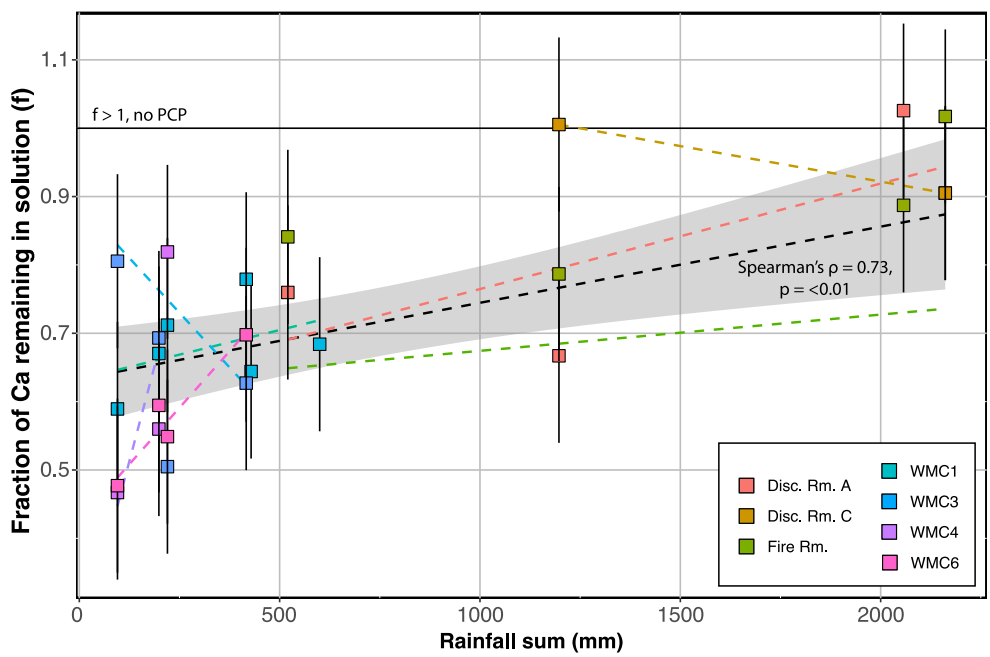

Figure 11. WMC and LSC modern calcite *f* versus the amount of rainfall that fell during the interval when the calcite formed. The colored dashed lines show linear regressions for individual drip sites and the black dashed line shows the linear regression for the combined WMC and LSC data sets.

and rainfall amounts. However, for example, the highest *f* value corresponds to the third largest rainfall sum. Sites WMC4 and WMC6 are deeper in the cave and display steeper slopes than WMC1, which is consistent with these sites experiencing longer flow paths through the vadose zone and more variability in PCP. Site WMC3 is closest to the modern cave entrance, produces a lower α than other WMC sites, and shows a negative relationship with rainfall, including producing the highest *f* value for the site during the driest interval when the other sites indicate the least amount of PCP respectively, indicating that it may not be a reliable recorder of PCP. At LSC, the Fire Room and Discovery Room A display generally positive relationships with rainfall, with the rainiest intervals corresponding to *f* values that are close to 1, indicating little to no PCP (Figure 11). The two modern calcite samples from Discovery Room C produce *f* values of 1.00 and 0.91 for rainfall sums of 1,197 and 2,161 mm, respectively, which may indicate that these rainfall amounts are sufficient to produce little to no PCP at this site. At LSC, the reconstruction of *f* values close to 1 for the wettest intervals points to an upper rainfall threshold above which little to no PCP occurs. This is useful for constraining interpretations of *f* values close to 1 in speleothem records, which should be considered minimum estimates of paleo-rainfall (de Wet et al., 2021).

These comparisons demonstrate that an inverse relationship between rainfall and PCP may be resolvable at seasonal to monthly scales, though there is variability in this relationship within the cave systems. This variability in PCP reconstructions between coeval measurements from different drip sites points to complexities in the ways that water infiltration paths respond to rainfall and/or in the way that speleothems record PCP variability within the same cave system. For example, the moisture status of the soil and vadose zone prior to a large rainfall event may impact the degree of infiltration and flow rate, with implications for PCP, but this is difficult to constrain in the field. It may be the case that PCP signals recorded by speleothem $\delta^{44}Ca$ are most representative of large magnitude variability in rainfall on multi-year timescales, as is shown by the comparison between PCP at the drier WMC site relative to LSC, which is wetter. This framework is consistent with findings from Li et al. (2018) who found speleothem $\delta^{44}Ca$ correlated most strongly with decadal-scale periods of aridity at Heshang Cave. In this case, longer term monitoring studies will be necessary to fully constrain and identify the relationship between rainfall, PCP, and cave system $\delta^{44}Ca$. In order to develop semi-quantitative estimates of paleo-rainfall rates from fossil speleothem $\delta^{44}Ca$ most robustly, it will be important to calibrate cave monitoring data with multiple coeval measurements of PCP and rainfall, ideally spanning a large range of rainfall amounts. This should be a focus of cave monitoring studies that utilize $\delta^{44}Ca$ moving forward.

5. Conclusions

In this study, we present measurements of $\delta^{44}Ca$, $\delta^{13}C$, and trace element ratios (Mg/Ca, Sr/Ca, Ba/Ca) from drip waters, modern calcite speleothems, and carbonate host rocks from two California cave systems that span climatological and geologic gradients. Measured $\delta^{44}Ca$ values in both drip waters and modern calcite are consistent with PCP-driven enrichment in cave samples relative to host rock $\delta^{44}Ca$ signatures. Drip water and modern calcite $\delta^{44}Ca$ tends to correlate with trace element ratios at WMC, which points to a shared PCP control on these proxies. Calcium isotopic values do not tend to correlate with other geochemical data at LSC, indicating that PCP may not act as a straightforward and singular control for all these other proxies at this site. Greater enrichment in the heavier ^{44}Ca isotope in drip waters and modern calcite is associated with deeper sites at WMC, indicating that longer flow paths allow for more PCP under the same hydroclimate conditions.

Cave system $\delta^{44}Ca$ can be used to model PCP, which can be linked to changes in local rainfall (de Wet et al., 2021; Li et al., 2018; Owen et al., 2016). This new proxy may also help elucidate and account for non-PCP related controls on other moisture-sensitive proxies, such as the contribution of soil components or incongruent dissolution of host rock phases (Lechleitner et al., 2021; Stoll et al., 2023). However, our work shows that cave system $\delta^{44}Ca$ variability may also be impacted by non-PCP factors, such as variability in the host rock $\delta^{44}Ca$ signature, and by factors that exert a secondary, non-climate related influence on PCP, such as depth from the surface and flow path type. Using the Rayleigh fractionation model framework, we calculated the amount of PCP experienced by infiltrating waters at multiple drip sites within both cave systems. Drip water and modern calcite $\delta^{44}Ca$ data from WMC suggest that this cave experiences ~20% more PCP than LSC, which is consistent with the difference in rainfall measurements at these sites. We observe an overall inverse relationship between PCP amount and rainfall sum, though this relationship is variable across individual sites within each cave, with some WMC and LSC sites indicating a strong rainfall control on PCP, while other sites in the same cave show a more equivocal response. Additional long-term monitoring studies of cave system $\delta^{44}Ca$ variability will be crucial for

further constraining the relationship between PCP and rainfall across different cave sites, with important implications for how best to generate quantitative estimates of past rainfall changes using speleothems.

Conflict of Interest

The authors declare no conflicts of interest relevant to this study.

Data Availability Statement

The data presented in this study are shown in Table S1 of the Supporting Information S1 and Table S2 and are available for download from the NOAA National Centers for Environmental Information Paleoclimate Data repository (https://www.ncei.noaa.gov/products/paleoclimatology).

Acknowledgments
Funding was provided by the National Science Foundation (AGS-1554998 and AGS-2202883) and the National Geographic Society (NGS-39815) (to Jessica L. Oster), the Karst Waters Institute, the Cave Research Foundation, the Geological Society of America, and the National Speleological Society (to Cameron B. de Wet), and the National Science Foundation (EAR-2202851) (to Elizabeth M. Griffith). We thank Mike Davis of the Western Cave Conservancy, Susan Petrie of the Peninsula Open Space Trust, and Dave Mundt and the Lake Shasta Caverns staff for their support in the field. We also thank reviewers Heather Stoll and Christopher Day for their helpful comments and suggestions.

References

Arguez, A., Durre, I., Applequist, S., Squires, M., Russell, V., Yin, X., & Bilotta, R. (2010). *NOAA's U.S. climate normals (1981-2010)*. NOAA National Centers for Environmental Information. https://doi.org/10.7289/V5PN93JP

Cheng, H., Edwards, R., Sinha, A., Spötl, C., Yi, L., Chen, S., et al. (2016). The Asian monsoon over the past 640,000 years and ice age terminations. *Nature*, *534*(7609), 640–646. https://doi.org/10.1038/nature18591

Coplen, T. B. (1998). A manual for a Laboratory Information Management System (LIMS) for light stable isotopes. (Version 7.0). *Open-File Report*. https://doi.org/10.3133/ofr98284

Day, C. C., & Henderson, G. M. (2013). Controls on trace-element partitioning in cave-analogue calcite. *Geochimica et Cosmochimica Acta*, *120*, 612–627. https://doi.org/10.1016/j.gca.2013.05.044

Demirmen, F., & Harbaugh, J. W. (1965). Petrography and origin of Permian McCloud Limestone of northern California. *Journal of Sedimentary Research*, *35*(1), 136–154. https://doi.org/10.1306/74D7120D-2B21-11D7-8648000102C1865D

Dettinger, M. (2011). Climate change, atmospheric rivers, and floods in California—A multimodel analysis of storm frequency and magnitude changes[1]. *JAWRA Journal of the American Water Resources Association*, *47*(3), 514–523. https://doi.org/10.1111/j.1752-1688.2011.00546.x

de Wet, C. (2023). *A multi-pronged approach to understanding moisture dynamics in North America since the Last Interglacial using proxy records and climate model output. Doctoral Dissertation*. Vanderbilt University. Vanderbilt University Institutional Repository.

de Wet, C. B., Erhardt, A. M., Sharp, W. D., Marks, N. E., Bradbury, H. J., Turchyn, A. V., et al. (2021). Semiquantitative estimates of rainfall variability during the 8.2 kyr event in California using speleothem calcium isotope ratios. *Geophysical Research Letters*, *48*(3), 1–11. https://doi.org/10.1029/2020GL089154

Fairchild, I. J., & Treble, P. C. (2009). Trace elements in speleothems as recorders of environmental change. *Quaternary Science Reviews*, *28*(5), 449–468. https://doi.org/10.1016/j.quascirev.2008.11.007

Fantle, M. S., & DePaolo, D. J. (2005). Variations in the marine Ca cycle over the past 20 million years. *Earth and Planetary Science Letters*, *237*(1), 102–117. https://doi.org/10.1016/j.epsl.2005.06.024

Fohlmeister, J., Voarintsoa, N. R. G., Lechleitner, F. A., Boyd, M., Brandtstätter, S., Jacobson, M. J., & Oster, J. (2020). Main controls on the stable carbon isotope composition of speleothems. *Geochimica et Cosmochimica Acta*, *279*, 67–87. https://doi.org/10.1016/j.gca.2020.03.042

Gabitov, R. I., Sadekov, A., & Leinweber, A. (2014). Crystal growth rate effect on Mg/Ca and Sr/Ca partitioning between calcite and fluid: An in situ approach. *Chemical Geology*, *367*, 70–82. https://doi.org/10.1016/j.chemgeo.2013.12.019

Giesche, A., Hodell, D., Petrie, C., Haug, G., Adkins, J., Schröder, B., et al. (2023). Recurring summer and winter droughts from 4.2-3.97 thousand years ago in North India. *Communications Earth & Environment*, *4*(1), 1234567890. https://doi.org/10.1038/s43247-023-00763-z

Griffith, E. M., Schauble, E. A., Bullen, T. D., & Paytan, A. (2008). Characterization of calcium isotopes in natural and synthetic barite. *Geochimica et Cosmochimica Acta*, *72*(23), 5641–5658. https://doi.org/10.1016/j.gca.2008.08.010

Griffith, E. M., Schmitt, A.-D., Andrews, M. G., & Fantle, M. S. (2020). Elucidating modern geochemical cycles at local, regional, and global scales using calcium isotopes. *Chemical Geology*, *534*, 119445. https://doi.org/10.1016/j.chemgeo.2019.119445

Gussone, N., Böhm, F., Eisenhauer, A., Dietzel, M., Heuser, A., Teichert, B. M. A., et al. (2005). Calcium isotope fractionation in calcite and aragonite. *Geochimica et Cosmochimica Acta*, *69*(18), 4485–4494. https://doi.org/10.1016/j.gca.2005.06.003

Hart, E. W., & Williams, J. W. (1978). Geologic review process. *California Geology*, *31*(10), 235–236.

Heuser, A., Schmitt, A. D., Gussone, N., & Wombacher, F. (2016). Analytical methods. In *Calcium stable isotope geochemistry. Advances in isotope geochemistry*. Springer. https://doi.org/10.1007/978-3-540-68953-9_2

Hu, C., Henderson, G. M., Huang, J., Xie, S., Sun, Y., & Johnson, K. R. (2008). Quantification of Holocene Asian monsoon rainfall from spatially separated cave records. *Earth and Planetary Science Letters*, *266*(3–4), 221–232. https://doi.org/10.1016/j.epsl.2007.10.015

Huang, Y., & Fairchild, I. J. (2001). Partitioning of Sr^{2+} and Mg^{2+} into calcite under karst-analogue experimental conditions. *Geochimica et Cosmochimica Acta*, *65*(1), 47–62. https://doi.org/10.1016/S0016-7037(00)00513-5

Lachniet, M. (2009). Climatic and environmental controls on speleothem oxygen-isotope values. *Quaternary Science Reviews*, *28*(5–6), 412–432. https://doi.org/10.1016/j.quascirev.2008.10.021

Lechleitner, F. A., Day, C. C., Kost, O., Wilhelm, M., Haghipour, N., Henderson, G. M., & Stoll, H. M. (2021). Stalagmite carbon isotopes suggest deglacial increase in soil respiration in western Europe driven by temperature change. *Climate of the Past*, *17*(5), 1903–1918. https://doi.org/10.5194/cp-17-1903-2021

Lehn, G. O., Jacobson, A. D., & Holmden, C. (2013). Precise analysis of Ca isotope ratios ($\delta^{44}/^{40}$Ca) using an optimized ^{43}Ca–^{42}Ca double-spike MC-TIMS method. *International Journal of Mass Spectrometry*, *351*, 69–75. https://doi.org/10.1016/j.ijms.2013.06.013

Li, X., Cui, X., He, D., Liao, J., & Hu, C. (2018). Evaluation of the Heshang Cave stalagmite calcium isotope composition as a paleohydrologic proxy by comparison with the instrumental precipitation record. *Scientific Reports*, *8*(1), 2615. https://doi.org/10.1038/s41598-018-20776-5

Magiera, M., Lechleitner, F. A., Erhardt, A. M., Hartland, A., Kwiecien, O., Cheng, H., et al. (2019). Local and regional Indian summer monsoon precipitation dynamics during termination II and the last interglacial. *Geophysical Research Letters*, *46*(21), 12454–12463. https://doi.org/10.1029/2019GL083721

Medina-Elizalde, M., Burns, S. J., Lea, D. W., Asmerom, Y., von Gunten, L., Polyak, V., et al. (2010). High resolution stalagmite climate record from the Yucatán Peninsula spanning the Maya terminal classic period. *Earth and Planetary Science Letters*, *298*(1), 255–262. https://doi.org/10.1016/j.epsl.2010.08.016

Mucci, A., & Morse, J. W. (1983). The incorporation of Mg^{2+} and Sr^{2+} into calcite overgrowths: Influences of growth rate and solution composition. *Geochimica et Cosmochimica Acta*, *47*(2), 217–233. https://doi.org/10.1016/0016-7037(83)90135-7

Oster, J. L., Covey, A. K., Lawrence, C. R., Giannetta, M. G., & Druhan, J. L. (2021). A reactive transport approach to modeling cave seepage water chemistry II: Elemental signatures. *Geochimica et Cosmochimica Acta*, *311*, 353–373. https://doi.org/10.1016/j.gca.2021.06.040

Oster, J. L., Sharp, W. D., Covey, A. K., Gibson, J., Rogers, B., & Mix, H. (2017). Climate response to the 8.2 ka event in coastal California. *Scientific Reports*, *7*(1), 3886. https://doi.org/10.1038/s41598-017-04215-5

Oster, J. L., Weisman, I. E., & Sharp, W. D. (2020). Multi-proxy stalagmite records from northern California reveal dynamic patterns of regional hydroclimate over the last glacial cycle. *Quaternary Science Reviews*, *241*, 106411. https://doi.org/10.1016/j.quascirev.2020.106411

Owen, R. A., Day, C. C., Hu, C. Y., Liu, Y. H., Pointing, M. D., Blättler, C. L., & Henderson, G. M. (2016). Calcium isotopes in caves as a proxy for aridity: Modern calibration and application to the 8.2 kyr event. *Earth and Planetary Science Letters*, *443*, 129–138. https://doi.org/10.1016/j.epsl.2016.03.027

PRISM Climate Group. (2021). *PRISM climate group*. Oregon State University. Retrieved from https://prism.oregonstate.edu/

Reynard, L. M., Day, C. C., & Henderson, G. M. (2011). Large fractionation of calcium isotopes during cave-analogue calcium carbonate growth. *Geochimica et Cosmochimica Acta*, *75*(13), 3726–3740. https://doi.org/10.1016/j.gca.2011.04.010

Serrato Marks, G., Medina-Elizalde, M., Burns, S., Weldeab, S., Lases-Hernandez, F., Cazares, G., & McGee, D. (2021). Evidence for decreased precipitation variability in the Yucatán Peninsula during the Mid-Holocene. *Paleoceanography and Paleoclimatology*, *36*(5), e2021PA004219. https://doi.org/10.1029/2021PA004219

Sherwin, C., & Baldini, J. (2011). Cave air and hydrological controls on prior calcite precipitation and stalagmite growth rates: Implications for palaeoclimate reconstructions using speleothems. *Geochimica et Cosmochimica Acta*, *75*(14), 3915–3929. https://doi.org/10.1016/j.gca.2011.04.020

Sinclair, D. J., Banner, J. L., Taylor, F. W., Partin, J., Jenson, J., Mylroie, J., et al. (2012). Magnesium and strontium systematics in tropical speleothems from the western Pacific. *Chemical Geology*, *294–295*, 1–17. https://doi.org/10.1016/j.chemgeo.2011.10.008

Stoll, H. M., Day, C., Lechleitner, F., Oliver, K., Endres, L., Sliwinski, J., et al. (2023). Distinguishing the vegetation and soil component of $\delta^{13}C$ variation in speleothem records from degassing and prior calcite precipitation effects. *Climate of the Past*, *19*(12), 2423–2444. https://doi.org/10.5194/cp-19-2423-2023

Stoll, H. M., Müller, W., & Prieto, M. (2012). I-STAL, a model for interpretation of Mg/Ca, Sr/Ca and Ba/Ca variations in speleothems and its forward and inverse application on seasonal to millennial scales. *Geochemistry, Geophysics, Geosystems*, *13*(9), Q09004. https://doi.org/10.1029/2012GC004183

Tang, J. W., Dietzel, M., Bohm, F., Kohler, S. J., & Eisenhauer, A. (2008). Sr^{2+}/Ca^{2+} and $^{44}Ca/^{40}Ca$ fractionation during inorganic calcite formation: II. Ca isotopes. *Geochimica et Cosmochimica Acta*, *72*(15), 3733–3745. https://doi.org/10.1016/j.gca.2008.05.033

Tesoriero, A. J., & Pankow, J. F. (1996). Solid solution partitioning of Sr^{2+}, Ba^{2+}, and Cd^{2+} to calcite. *Geochimica et Cosmochimica Acta*, *60*(6), 1053–1063. https://doi.org/10.1016/0016-7037(95)00449-1

Tremaine, D. M., & Froelich, P. N. (2013). Speleothem trace element signatures: A hydrologic geochemical study of modern cave dripwaters and farmed calcite. *Geochimica et Cosmochimica Acta*, *121*, 522–545. https://doi.org/10.1016/j.gca.2013.07.026

Warken, S. F., Fohlmeister, J., Schröder-Ritzrau, A., Constantin, S., Spötl, C., Gerdes, A., et al. (2018). Reconstruction of late Holocene autumn/winter precipitation variability in SW Romania from a high-resolution speleothem trace element record. *Earth and Planetary Science Letters*, *499*, 122–133. https://doi.org/10.1016/j.epsl.2018.07.027

Warken, S. F., Scholz, D., Spötl, C., Jochum, K. P., Pajón, J. M., Bahr, A., & Mangini, A. (2019). Caribbean hydroclimate and vegetation history across the last glacial period. *Quaternary Science Reviews*, *218*, 75–90. https://doi.org/10.1016/j.quascirev.2019.06.019

Wassenburg, J. A., Riechelmann, S., Schröder-Ritzrau, A., Riechelmann, D. F. C., Richter, D. K., Immenhauser, A., et al. (2020). Calcite Mg and Sr partition coefficients in cave environments: Implications for interpreting prior calcite precipitation in speleothems. *Geochimica et Cosmochimica Acta*, *269*, 581–596. https://doi.org/10.1016/j.gca.2019.11.011

Wogsland, B. V. (2020). *Organomineralization of microbialites from Storr's Lake, San Salvador Island, Bahamas: Calcium stable isotope analysis using TIMS and a ^{42}Ca-^{43}Ca double spike*. The Ohio State University. Retrieved from http://rave.ohiolink.edu/etdc/view?acc_num=osu1587723502946554

Wong, C. I., & Breecker, D. O. (2015). Advancements in the use of speleothems as climate archives. *Quaternary Science Reviews*, *127*, 1–18. https://doi.org/10.1016/j.quascirev.2015.07.019

Wright, K. T., Johnson, K. R., Bhattacharya, T., Marks, G. S., McGee, D., Elsbury, D., et al. (2022). Precipitation in northeast Mexico primarily controlled by the relative warming of Atlantic SSTs. *Geophysical Research Letters*, *49*(11), e2022GL098186. https://doi.org/10.1029/2022GL098186

Xue, G., Cai, Y., Lu, Y., Ma, L., Cheng, X., Liu, C., et al. (2021). Speleothem-based hydroclimate reconstructions during the penultimate deglaciation in northern China. *Paleoceanography and Paleoclimatology*, *36*(4), e2020PA004072. https://doi.org/10.1029/2020PA004072